Full length Article

Age and nature of Triassic magmatism in the Netoni Intrusive Complex, West Papua, Indonesia

Max Webb, Lloyd T. White

PII: S1367-9120(16)30298-X
DOI: http://dx.doi.org/10.1016/j.jseaes.2016.09.019
Reference: JAES 2819

To appear in: *Journal of Asian Earth Sciences*

Received Date: 28 May 2016
Revised Date: 26 September 2016
Accepted Date: 28 September 2016

Please cite this article as: Webb, M., White, L.T., Age and nature of Triassic magmatism in the Netoni Intrusive Complex, West Papua, Indonesia, *Journal of Asian Earth Sciences* (2016), doi: http://dx.doi.org/10.1016/j.jseaes.2016.09.019

Age and nature of Triassic magmatism in the Netoni Intrusive Complex, West Papua, Indonesia

Max Webb[1*] and Lloyd T. White[1]

1. Southeast Asia Research Group, Department of Earth Sciences, Royal Holloway University of London, Egham, Surrey, TW20 0EX

*Corresponding Author: Max Webb (email: max.cm.webb@gmail.com)

ABSTRACT

We report field observations together with petrological, geochemical and geochronological data from granitoids of the Netoni Intrusive Complex of West Papua. Until now, our knowledge of the timing of granitic magmatism in this region has been limited to a wide range of ages (241–6.7 Ma) obtained from K-Ar measurements of hornblende, biotite and plagioclase, primarily from samples of river detritus. We collected *in situ* samples along several traverses into the intrusive complex to: (1) develop a better understanding of the lithologies within the intrusive complex; and (2) determine the timing of magmatism using U-Pb dating of zircon. We also dated zircons from two river sand samples to identify other potential pulses of magmatism that may have been missed due to a sampling bias. The zircons extracted from the river sands yield age spectra similar to those obtained from the *in situ* samples. The combined data demonstrate that magmatism in the Netoni Intrusive Complex occurred between 248 Ma and 213 Ma. The petrological and geochemical data indicate that the granitoids were most likely emplaced in an ocean-continent (Andean style) subduction setting. This builds on previous work which suggests that a magmatic belt extended along eastern Gondwana (now New Guinea and eastern Australia) throughout much of the Paleozoic. The volcanic ejecta that were produced along this arc and the subsequent erosion of the mountain chain are a potential source of detritus for Triassic and younger sedimentary rocks in New Guinea, eastern Indonesia and north/northwestern Australia.

Keywords: Bird’s Head, granite, zircon, geochronology, tectonics, geochemistry

1. INTRODUCTION

The Bird's Head Peninsula is the north-westernmost component of New Guinea and represents a long-lived plate boundary between the Australian Plate and the Caroline, Philippine Sea and Pacific plates (e.g. Hamilton, 1979; Dow & Sukamto, 1984; Audley-Charles, 1988; 1991; Metcalfe, 1990; Charlton, 2001; Hall, 2002; Hill & Hall, 2003; Hall 2012). Much of what we know about the geology of this complicated region stems from field campaigns conducted by Dutch geologists (summarised in Visser & Hermes, 1962) as well as a joint mapping campaign conducted by Indonesian and Australian geologists in the 1970's and 80's (e.g. Pieters et al., 1979; 1983; Dow et al., 1988). The majority of subsequent work has focused on hydrocarbon exploration in the Salawati and Bintuni Basins (e.g. Chevallier & Bordenave, 1986; Phoa & Samuel, 1986; Perkins & Livsey, 1993; Charlton, 1996) or much further south in the Lengguru Fold and Thrust Belt (e.g. Bailly et al., 2009). All of this work has led to a range of tectonic models to explain the evolution of western New Guinea. For instance, many consider that the Bird's Head has been part of the northern margin of the Australian Plate from the Paleozoic to the present day, with varying amounts of rotation proposed (Hamilton, 1979; Dow & Sukamto, 1984; Audley-Charles, 1988; 1991; Metcalfe, 1990; Charlton, 2001; Hall, 2002; Hill & Hall, 2003). Others propose that the Bird's Head is a separate micro-continent that was translated from eastern to western New Guinea (Pigram & Pangabbean, 1984; Giddings et al., 1993; Struckmeyer et al., 1993). It is clear that more data are required to test such models, particularly new geochronological data from the Bird's Head region. This is because our knowledge of the timing of magmatic and metamorphic events is based on a compilation of K-Ar dating of predominantly river detritus that was collected as part of the joint Indonesian/Australian government mapping

campaign (compiled by Bladon, 1988). We now have access to a much broader range of isotopic dating methods that are arguably more suitable for determining the age of magmatic and metamorphic events. For instance, U-Pb data were recently obtained from zircons extracted from the volcanoclastic sediments of the Tipuma Formation (Gunawan et al., 2012; 2014). This work showed that the Tipuma Formation contained a significant population of Permo-Triassic zircons that were considered to represent ash fall from a volcanic arc active during the Triassic.

We therefore present several U-Pb zircon ages from granitoids in a suite referred to as the Netoni Intrusive Complex (Pieters et al., 1983). Our aim is to determine whether the erosion of this intrusive complex might explain the similar age spectra as have been reported in the Tipuma Formation (e.g. Gunawan et al., 2012; 2014) and potentially further afield in eastern Indonesia (e.g. Zimmerman and Hall, 2016). We also report new geochemical and petrological data from the Netoni Intrusive Complex and consider these alongside the U-Pb data to develop a better understanding of the petrogenesis of these magmatic rocks.

2. REGIONAL GEOLOGY

The oldest rocks that are exposed in the Bird's Head Peninsula consist of Silurian to Devonian metasedimentary rocks termed the Kemum Formation (Visser & Hermes, 1962; Pieters et al., 1983). These are considered to represent distal turbidites that were deposited at the northern edge of the Australian continent, eastern Gondwana and were deformed and metamorphosed during the Devonian or Early to Middle Carboniferous (Pieters et al., 1983, Dow et al., 1988). These metasedimentary rocks are cross-cut by Late Carboniferous and Permo-Triassic granitic intrusions (Pieters et

al., 1983) that are generally coeval with the Netoni Intrusive Complex. These Carboniferous-Triassic granitoids found throughout New Guinea are considered to have been generated in an Andean style volcanic arc system that extended along the northern margin of New Guinea and southward along eastern Australia (Metcalfe, 1998; Charlton 2001; Hill & Hall, 2003; Gunawan et al., 2012; 2014).

The Netoni Intrusive Complex[1] (also known as the Netoni Fragment) is found in the Tamrau Mountains in the north of the Bird's Head (Fig. 1). It has not been widely studied. It was first described as a large granitoid body north of the Sorong Fault Zone (Pieters et al., 1979). Detailed field relationships and petrographic results were later reported in Pieters et al., (1983; 1989) together with preliminary K-Ar age data (Bladon 1988). No further work has since been conducted.

Pieters et al., (1983; 1989) reported that the intrusive complex consists of medium- to coarse-grained granitoids including; I-type monzonite to granite (with abundant biotite and hornblende as well as rare pyroxene and muscovite), quartz diorite to diorite and pegmatite, along with gabbro, amphibolite and metasedimentary xenoliths. The pegmatite is considered to represent a late phase within the intrusive complex and, along with the xenoliths, are principally found along the margins of the complex (Pieters et al., 1983; 1989).

[1] The Netoni Intrusive Complex was presumably named after one of the dominant peaks (Gunung Netoti) in the mountain range where it is situated (Tamrau Mountains). Note, however that the mountain is referred to as *Netoti*, not *Netoni*, but for the sake of continuity we also refer to this as the Netoni Intrusive Complex.

The intrusive complex is considered to have been emplaced between 241 Ma and 208 Ma according to several K-Ar ages obtained from plagioclase, biotite, and hornblende extracted from various river float samples (Bladon, 1988). Pieters et al. (1983) originally proposed a slightly different interpretation of the same K-Ar age data, suggesting that the Netoni Intrusive Complex was emplaced between 245 Ma and 221 Ma. To confuse matters further, a series of younger ages (Jurassic to Neogene) were also obtained from these rocks (Table 3) (Bladon, 1988). The youngest age (6.7 Ma) however was obtained from amphibolite float and was interpreted to represent a more recent thermal event, most likely associated with post-crystallisation deformation of the granitoids (Bladon, 1988; Pieters et al., 1989). This deformation is evident in different parts of the batholith and explains why it has been mapped as an almost entirely fault bounded allochthonous block (Dow et al., 1988). Its southern boundary is delineated by the Sorong Fault Zone, which cuts between the Netoni Intrusive Complex and the Kemum Formation (Visser & Hermes, 1962; Pieters et al., 1983) (Fig. 2a). To the north various curvilinear faults separate the intrusive complex from the Tamrau Formation (Pieters et al., 1989) (Fig. 2a). It is only the western edge of the complex that is not faulted; here it is instead overlain by the Late Cretaceous Amiri Sandstone (Pieters et al., 1989) (Fig. 2a). Components of the Netoni Intrusive Complex are also entrained within bisecting fault segments of the Sorong Fault Zone (Pieters et al., 1989).

3. METHODOLOGY

3.1 Field Observations

Two river traverses were examined along the southern boundary of the Netoni Intrusive Complex (Fig. 2a). The first traverse was directed northwards into the southern margin of the intrusive complex (Fig. 2b), while the second was conducted in a river that runs broadly parallel to its southern edge (Fig. 2c). We also sampled along a road that sections the eastern end of the intrusive complex (Fig. 2a). Each of these traverses provided different insights. The first traverse revealed details about intrusive relationships between the granitic rocks and the surrounding meta-sedimentary country rocks; the second traverse cut through predominantly meta-sedimentary country rock; and the road cut exposed a ~100 m section of fractured granitoids with metasedimentary xenoliths and roof pendants. Samples were collected along each traverse for petrographical, geochemical and U-Pb isotopic analyses.

3.2 Geochemical Analyses

Seven granite samples showing little to no alteration were crushed into 2-5 cm^3 pieces and any aggregate showing weathered surfaces were removed. The remaining aggregate was washed and sieved to remove potential contaminants from the jaw crusher and dried before being ground into a fine-powder using a TEMA tungsten carbide swing mill at Royal Holloway University of London (RHUL). The samples were quartered and an aliquot was set aside to be pulverised further for major and trace element geochemical analyses using a 2010 PANalytical Axios sequential X-ray fluorescence spectrometer at RHUL. Major elements were analysed on fusion disks prepared from sample powder ignited at 1100°C, providing the loss on ignition (LOI) value (Table 2). Trace elements were analysed on pressed 40mm pellets with matrix

corrections calculated from the major element composition, and calibrated to 40 international standards. Limits of detection (LoD) were calculated for the major and trace elements using long-term data collected using the same equipment (cf. https://www.royalholloway.ac.uk/earthsciences/labs/xrf.aspx – last accessed 14.09.2016).

3.3 U-Pb dating of zircon

Zircons were extracted from five granites and two river sands from within the Netoni Intrusive Complex. This was achieved by processing <250 μm milled aggregate with a Wilfley Table, heavy density liquids and a Frantz Isodynamic separator at RHUL. Zircons from each sample were mounted in epoxy resin and later polished to expose the mid-section of each grain. The resin stubs were then photographed under transmitted light to determine the location of cracks and inclusions within the zircon grains. Cathodoluminescence (CL) images were also obtained using a Hitachi S3000 scanning electron microscope at RHUL to image any internal growth zones within the zircons that might be targeted using laser ablation inductively coupled plasma mass spectrometry (LA-ICP-MS).

U-Pb isotopic data were collected using an ESI NWR 193 mm laser ablation system coupled to an Agilent 7700 quadrupole-based ICP-MS at the London Geochronology Centre (LGC), University College London (UCL). The analyses were collected during two analytical sessions. The instrument parameters were kept the same between each session and between each analysis. The LA-ICP-MS parameters are largely the same as those adopted by Jackson et al., (2004) and further details are provided in Supplementary Data File 1.

Plešovice zircon (337.13±0.37 Ma: Slama et al., 2008) was used as an external age standard to correct for mass bias and down-hole fractionation. NIST SRM 612 glass (Reed, 1992; Jochum et al., 2011) was used as an external trace element concentration standard. Three Plešovice zircons were measured at the beginning and end of each session and between each change of sample. Another two Plešovice standards were measured between every ~40 unknown analyses. Three measurements of NIST SRM 612 glass were collected at the beginning of the analytical session with another two measurements collected at the end. In addition, measurements of the TEMORA 2 zircon (416.75±0.24 Ma – Black et al., 2004) were made at the same intervals as the Plešovice zircon standard to qualitatively assess the accuracy of the data collected and to study the effects of laser drift and down-hole fractionation. LA-ICP-MS data were reduced using Iolite 2.5 (Paton et al., 2010; 2011) with the VizualAge data reduction scheme (Petrus & Kamber, 2012). This allowed the identification of any non-zircon grains or cases in which the laser continued firing into the underlying epoxy. Additionally, the program allowed for identification of the most appropriate down-hole fractionation model to be applied based on the signal behavior of the Plešovice standards (in this case an exponential fit was applied). Laser drift was modelled against the Plešovice and secondary TEMORA 2 grains and this was used to produce a propagated error for each analysis.

We then refined the data obtained for each sample by omitting individual analyses from further interpretation if they were:

1. Suspected of being obtained from a mixture of zircon and epoxy resin.

2. ≥ 10% discordant (based on the U^{238}/Pb^{206} vs. U^{235}/Pb^{207} isotopic systems).

All of the data points that were omitted from further interpretation according to the above qualifiers are highlighted in Supplementary Data File 2. Readers should also note that all results are reported using the $^{206}Pb/^{238}U$ isotopic system (as no ages >800 Ma were obtained from these samples).

The location of each LA-ICP-MS analysis was compared with the CL imagery to determine if particular age results corresponded with textural features (e.g. inherited zircon cores or metamorphic rims) (cf. Supplementary Data File 3). However, we found no definitive correlation between zircon age and morphology. We also compared the uranium concentration with the apparent age of each ablation site to identify matrix effects associated with metamictisation (e.g. Allen & Campbell 2012; White & Ireland 2012), but found no correlation between age and U concentration (Supp. Data 2).

The Microsoft Excel macro Isoplot (version 4.1 - Ludwig, 2009) was used for further calculations and data visualisation with various plots. Tera-Wasserburg plots (Tera & Wasserburg, 1972) were used to display all concordant data for individual analyses. The accepted age data for each granite sample were plotted on probability density and weighted mean plots. A weighted mean age was calculated for samples where only one clear age population was present. Outliers were rejected from the weighted mean age calculation if they fell outside a 95% confidence limit (i.e. >1.96σ). For samples with more than one age population, we used the unmix age function of Isoplot which

uses a mixture modeling approach to determine the ages and proportions of distinct components within a zircon age data set based on the analytical uncertainties (Sambridge & Compston, 1994). This is best applied with user input on the number of distinct age populations and the relative proportion of analyses that define each population. We therefore followed a similar procedure to White et al., (2011) and used probability density plots to obtain estimates of the dominant age populations and the relative proportion of data within each age population.

4. RESULTS

4.1 Field Observations and Petrography

4.1.1 Metamorphic Country Rocks

The granitic rocks of the Netoni Intrusive Complex intruded a series of deformed medium- to high-grade gneiss, schist, phyllite, and amphibolite. The amphibolites typically occur as large pods intruded by granitic rocks (Fig. 3a). The higher-grade biotite-hornblende schists and garnet-sillimanite-biotite gneisses typically show lenses rich in ferromagnesian minerals surrounded by leucocratic, quartzo-feldspathic material (Fig. 3b-3d). Some of these rocks also contain abundant foliation-parallel pegmatites and 'pods' of leucocratic granite, which we assume represent deformed granite from the Netoni Intrusive Complex (Fig. 3c).

The high-grade gneisses likely originated from a pelitic alumino-silicate rich protolith and display a sillimanite zone prograde mineral assemblage (quartz-plagioclase-biotite-garnet-sillimanite). In thin section, gneissic banding is defined by 1-3 cm thick bands of biotite-rich melanosome (containing minor quartz, plagioclase, garnet, sillimanite and opaque minerals) and quartzo-feldspathic leucosome (containing

minor biotite and garnet) (Fig. 4a-b). Partially resorbed and recrystallised garnets with lobate to embayed grain boundaries are considered to have grown before or during deformation (Fig. 4a).

The biotite-hornblende schist is metamorphosed to amphibolite facies with the prograde mineral assemblage of quartz-plagioclase-muscovite-biotite-hornblende. Biotite (with subordinate muscovite) is concentrated in 1-2 cm thick lenses throughout the rock (Fig. 4c); however, hornblende is the dominant mineral and, together with biotite, defines the dominant schistosity.

The metamorphic country rocks show evidence of multiple phases of brittle and ductile deformation in some locations (e.g. River Traverse 2). This includes tight folds, extensional shear bands, and boudinaged quartz veins (Fig. 3d). Fault planes with offset markers display extensional (Fig. 3c) as well as strike-slip senses of movement. Extensional shear zones observed at outcrop scale are also observed in thin sections. These include symmetrically boudinaged quartz veins (Fig. 4d and 4e) as well as S/C/C' shear fabrics with displacements between 0.25 mm and 1.5 mm. Myrmekite textures are also observed in thin sections of the country rock (Fig. 4f), but were not observed in any of the granitic rocks. These textures may therefore be due to contact metamorphism associated with the intrusion of the Netoni granitoids.

Additionally, a range of other lithologies (e.g. calc-silicates/marbles, gabbro, serpentinite and sillimanite gneiss) were identified in river detritus along River Traverse 2 (Fig. 2c). We suspect that these rocks represent eroded material from phaccoids of the other lithostratigraphic units entrained within the Sorong Fault Zone.

4.1.2 Granitoids

The Netoni Intrusive Complex consists of equigranular, medium-grained (~0.75–4 mm) syeno-granite, monzo-granite and less abundant granodiorite (Table 1). We also found rare occurrences of porphyritic granite with ~2–5 cm K-feldspar phenocrysts and muscovite-rich pegmatite veins and cavities (Fig. 5a).

The granitoids generally occur as large exposures (~10 m^2) or as 30–50 cm dykes and <1.5 m pods within meta-sedimentary country rocks (Fig. 5b-c). We also observed 20–40 cm dykes and sills that passively intrude along foliation planes in the country rock (Fig. 3d) as well as multiple exposures of granite with several centimeter-to-several meter sized metasedimentary xenoliths (Fig. 5e). These include isolated roof pendants (Fig. 5f) as well as networks of granitic dykes and sills that segregate patches of metasedimentary country rock (Fig. 5d).

Thin sections of the syeno-granite and monzo-granite show that these are composed of quartz, plagioclase and K-feldspar along with minor (≤ 10%) biotite, muscovite and titanite (Fig. 6a-f) (Table 1). Similarly, the granodiorite contains minor (~10%) biotite and opaques alongside dominant quartz, plagioclase and K-feldspar. The majority of feldspars in the granitoids have undergone secondary alteration to white mica, with plagioclase apparently preferentially altered relative to the other feldspars. The biotite is commonly replaced by chlorite (Fig. 6f).

Many of the granitoids have experienced post-crystallisation deformation. This includes granitoids with centimeter scale east-west striking bands of protomylonite

and mylonite as well as a range of other microstructures including: sweeping undulose extinction, subgrain development, and bulging recrystallisation (BLG) in quartz (Fig. 6). The subgrains have elongate to 'chessboard' geometries (Fig. 6c) and quartz proto-ribbons define a weak fabric (Fig. 6d). The deformation of the granites likely occurred at low- to medium temperatures (~400°C) as is inferred from the bulging recrystallisation (e.g. Vernon, 2004; Trouw et al. 2009). The feldspars are less obviously deformed, but subgrain development and deformation lamellae occur in K-feldspar along with rare examples of kinked plagioclase (Fig. 6e-f). These are again indicative of deformation at low- to medium temperatures (400-500°C; Pryer, 1993; Passchier & Trouw, 1996).

4.2 Major and trace element geochemistry

Major element discrimination diagrams (Fig. 7 a–d) were used to classify the granite samples according to the results obtained from the XRF analyses (Table 2). The SiO_2 ranges from 74–78 wt. % for all samples and these all plot within the 'granite' field of the total alkali vs. silica diagram (TAS; Middlemost, 1994) (Fig. 7a). The modified alkali lime index (MALI; Frost et al., 2001) shows that the granites are alkali-calcic to calc-alkalic (Fig. 7b). The Fe Index plot (Miyashiro, 1970; Frost et al., 2001) indicates that four of the granite samples are ferroan and three are magnesian (Fig. 7c). The A/NK vs. ASI diagram (Shand, 1943; Zen, 1986; Frost et al., 2001) displays the peraluminous nature of all of the granite samples (Fig. 7d).

The trace element analyses of the granite samples were normalised to average continental crust (Rudnick & Gao, 2003) (Fig. 8a), primitive mantle (Palme &

O'Neill, 2003) (Fig. 8b) and ALL-MORB (Gale et al., 2013) (Fig. 8c) compositions, so these could be easily compared with trace element data obtained from other studies of granitoids in different geological settings. Relative to the average continental crust samples MW14-02, -03 and -11 are enriched in all trace elements with the exception of Cs, Ba, and Sr (Fig. 8a). Samples MW14-07, -08, -13 and -17 however, have enriched Rb, Th, U and Pb, with depleted Hf, Zr, Sr, and rare earth elements (REE) with respect to the average continental crust (Fig. 8a). All of the trace elements in the granitoids are enriched with respect to the primitive mantle (Fig. 8b), and when compared with MORB (Fig. 8c), the granitoids show prominent enrichment of Cs, Rb, Ba, Th, U, and Pb together with relatively lower or depleted concentrations of Nb and REE.

4.3 U-Pb Geochronology

4.3.1 Granites

Zircons were extracted from five granite samples for LA-ICP-MS U-Pb analyses. Ten to fifty zircons were analysed from each sample. The zircons are subhedral to euhedral and have elongate to stubby aspect ratios (Supplementary Data File 3). We also note that some of the grains are fragmented, which we suspect is due to the mineral separation procedures. Cathodoluminescence images show that the majority of grains have magmatic oscillatory and sector zoning (Supplementary Data File 3). In some cases these oscillatory zones overgrow older oscillatory zoned and homogeneous cores (Supplementary Data File 3).

4.3.2.1 Granite: MW14-17

Sample MW14-17 represents the oldest granite sample that was dated. Six analyses were omitted but another fifty-five analyses record ages between ~290 Ma and ~220 Ma (Fig. 9a). Examination of the probability density plots shows two distinct age populations (Supplementary Data File 3). The unmix age function identified the two age populations as 269.9 ± 1.8 Ma and 247.2 ± 1 Ma. These ages, plus their 2σ uncertainties have been displayed on the weighted average plots (Fig. 10a). We interpret the younger of these two ages (247.2 ± 1 Ma) to reflect the timing of crystallisation of this granite sample. Additionally the sample contains four older and five younger zircon ages which fall outside the uncertainty limits of the 'unmixed' ages (Fig. 10a). The older ages are interpreted to represent inheritance while the younger ages could reflect a subsequent thermal event after the crystallisation of the granite.

4.3.2.2 Granite: MW14-09

Twenty-nine zircons were analysed from the granite sample MW14-09. Only ten of these analyses were concordant (Fig. 9c). The concordant grains crystallised between ~230 Ma and ~250 Ma and yielded a weighted mean age of 242.9 ± 4.0 Ma (95% conf., MSWD 2.5, n = 9) (Fig. 10c). A single younger zircon (230.1 ± 7 Ma) falls outside the uncertainty limits of the weighted mean age and is interpreted to reflect a thermal event after crystallisation.

4.3.2.3 Granite: MW14-03

Thirty-eight zircons were analysed from the granite sample MW14-03. The majority of these analyses were concordant (Fig. 9d) and yielded ages between ~190 Ma and ~250 Ma. Examination of the probability density plots shows two distinct age

populations (Supplementary Data File 2) and these were defined using the unmix age function (243.0 ± 1.9 Ma and 229.2 ± 3.4 Ma) (Fig. 10d). We interpret the younger of these two ages (229.2 ± 3.4 Ma) to reflect the timing of granite crystallisation. Three anomalously young ages (186.1 ± 4.1 Ma, 192.1 ± 10 Ma, 197.7 ± 3.7 Ma) (Supplementary File 2) are considered to record the timing of a thermal event after the granite crystallised.

4.3.2.4 Granite: MW14-02

Thirty-five concordant zircons were analysed from the granite sample MW14-02 (Fig. 9e). These record crystallisation between ~205 Ma and ~240 Ma. The weighted mean age for this sample is 224.2 ± 2.1 Ma (95% conf., MSWD 1.1, n = 34). This is interpreted to reflect the timing of granite crystallisation (Fig. 10e). A single younger zircon age (208.4 ± 12 Ma) lies outside the weighted mean age uncertainty limits.

4.3.2.5 Granite: MW14-11

MW14-11 is the youngest granite sample that was dated from the Netoni Intrusive Complex. Thirty-seven concordant results were obtained from this sample (Fig. 9b). These grains crystallised between~195 Ma and ~230 Ma and yield a weighted mean age of 215.2 ± 1.9 Ma (95% conf., MSWD 0.7, n = 36) (Fig. 10b), which is interpreted as the timing of granite crystallisation. One of the analyses falls outside the weighted mean age uncertainty limits (195.4 ± 11 Ma) and is interpreted to reflect the timing of a post-crystallisation thermal event.

4.3.3 River Sands

River sand MW14-05 was sampled in the same N-S flowing river in which the main outcrop traverse through the Netoni Intrusive Complex was conducted (Figure 1). Ninety concordant grains were analysed from this sample and these crystallised between ~195 Ma and ~306 Ma (Fig. 11a). A dominant age peak of ~240 Ma corresponds directly with the magmatic crystallisation ages obtained from the *in situ* granite samples. An older grain (274 Ma) (LA-ICP-MS analysis: MW14-05_123) displays magmatic zonation and shares a similar age with inherited ages observed in MW14-17. However, the very large error (± 32 Ma) associated with this analysis makes this comparison quite speculative. Another analysis yields an age of 198 Ma (LA-ICP-MS analysis: MW14-05_89) and is comparable to the youngest grains that were recorded in MW14-03 and MW14-11.

The second river sand sample (MW14-14) was obtained from an E-W flowing river that samples along strike of the contact between the Netoni Intrusive Complex and the Sorong Fault Zone (Fig. 2c). The zircons in this sample record two distinct age peaks at ~220 Ma and ~245 Ma (Fig. 11b). This bi-modal age assemblage is comparable to ages obtained from the granitoids. A single younger age of 169.7 ± 7.2 Ma (MW14-14_31) is similar to results from the other river sand sample as well as many of the granitoids.

5. DISCUSSION

5.1 Petrogenesis of the Netoni Intrusive Complex

The granitoids that were observed in this study have a different mineralogy to those described in previous studies (Pieters et al., 1983; 1989), which included hornblende and rare pyroxene bearing granitoids. Our samples contain neither hornblende nor

pyroxene, only minor biotite and muscovite. This may reflect a sampling bias and variation in mineralogy across the Netoni Intrusive Complex. However, considering that Pieters et al., (1983; 1989) focussed largely on river float to describe the Netoni Intrusive Complex, it is possible that their hornblende/pyroxene granitoids were transported uncertain distances and instead reflect components of the Tamrau Formation or Moon Volcanics (Fig. 2a). The same might be said about gabbro or diorite xenoliths reported from within the Netoni Intrusive Complex (Pieters et al., 1989), as we also only observed these lithologies as detritus along River Traverse 2 (Fig. 2c).

Several hornblende schists and amphibolites were identified as being part of the Netoni Intrusive Complex in the earlier studies (Pieters et al., 1983; 1989). We interpret these to be xenoliths within the intrusive complex or components of the country rock (most likely metamorphosed Tamrau or Kemum Formation). This is based on our observations of granite-country rock interactions and that biotite-hornblende schist and garnet-sillimanite-biotite migmatite gneiss were found as xenoliths incorporated into the granites.

The presence of several metre length roof pendants, together with pegmatites, granite intrusion along country rock foliation planes, and evidence for country rock assimilation indicates that the exposures we observed represent the highest structural levels of the Netoni Intrusive Complex. At these levels the granite intrudes meta-sedimentary rocks within the upper continental crust, and lower temperatures (compared with the base of the intrusion) cause localised isolation of country rock xenoliths into the granitic melt.

The Netoni granitoids have calc-alkalic to alkali-calcic compositions (Figs. 7a) which are typically interpreted as partial melts generated in subduction zone and active continental margin settings (Pearce et al., 1984; Harris et al., 1986; Pearce, 1996). The fact that the Netoni granitoid compositions range from calc-alkalic to alkali-calcic might be due to differentiation or mixing of magmas from multiple sources (e.g. Frost et al., 2001). Differentiation of calcic tholeiitic magmas combined with contamination from silicic crustal material (e.g. assimilation and fractional crystallisation – AFC) can form both calc-alkalic and alkali-calcic granites (McDougall, 1962; Frost et al., 2001). The extensive incorporation of country rock xenoliths into the Netoni Intrusive Complex could well result in assimilation and fractional crystallisation if those xenoliths were to be partially or completely melted. Additionally the mildly peraluminous nature of the Netoni Intrusive Complex granites (Fig. 7d) would indicate input from alumina-rich country rocks via assimilation and removal of metaluminous phases (mainly hornblende) by fractional crystallisation. This process is commonly observed in continental margin subduction zones and areas of thickened crust (e.g. Brown et al., 1984).

Enhanced concentrations of Rb and Th relative to other trace elements (Ta, Nb, Hf, and Zr) particularly well observed when normalised to primitive mantle and ALL-MORB (Fig. 8b-c), indicate subduction zone enrichment of the lithospheric mantle (Hawkesworth, 1982; Brown et al., 1984). Additionally, enrichment in Rb, Ce, and La relative to primitive mantle (Fig. 8b) may be associated with contamination from the continental crust during assimilation and fractional crystallisation (Thorpe et al., 1984; Brown et al., 1984). Depletion in Sr and to a lesser degree Ba relative to

continental crust (which would typically be enriched in subduction related basalts and andesites) is explained by increased fractionation of plagioclase and alkali feldspar respectively (Brown et al., 1984). Finally, the marked peak in Pb and trough in Nb relative to ALL-MORB are indicative of subduction zone magmatism with Nb being preferentially retained within the subducted oceanic lithosphere (Wilson, 1989).

5.2 Geochronology

The geochronological data collected in this study indicate that the granitoids of the Netoni Intrusive Complex were emplaced during the Early to Late Triassic (248 Ma to 213 Ma). The intrusive complex most likely developed due to a series of pulses of activity as is reflected in the crystallisation ages obtained from the different granitoids (247.2 ± 1.0 Ma; 242.9 ± 4.0 Ma; 229.2 ± 3.4 Ma; 224.2 ± 2.1 Ma; 215.2 ± 1.9 Ma). These ages are broadly reflected in the age spectra of the river sand samples (Fig. 11). For instance, the 243.0 ± 1.9 Ma age population in MW14-03 correlates with the crystallisation ages obtained for sample MW14-17 and MW14-09. There is also evidence of inherited zircon in some of the granitoid samples. We suspect that these inherited zircons largely reflect recycling of slightly older igneous intrusions within the Netoni Intrusive Complex. There is no evidence of older (i.e. >300 Ma) inherited zircon in any of the granite samples (or river sands) that were dated. This is somewhat odd considering that the granitoids are largely peraluminous products that we have interpreted to reflect partial melting and assimilation of alumina-rich country rocks. We suspect this is due to partial melting of pelitic country rocks with no zircon, or very fine- grained zircon, where the majority of fine-grained zircons were assimilated in the melt.

Previous geochronology studies of the Netoni Intrusive Complex are restricted to several K-Ar ages on plagioclase, hornblende and biotite from samples of river detritus. These studies produced an array of ages from 241 - 6.7 Ma (Bladon, 1988) (Table 3). Several of these K-Ar ages correlate with the Early-Late Triassic ages produced by U-Pb zircon geochronology in this study (Table 3). Several younger ages are also recorded in the U-Pb and K-Ar systems (particularly the ~190 Ma zircon ages observed in samples MW14-03 & MW14-11). We suspect that these could record post-crystallisation thermal events that pass the closure temperatures of the minerals in question (e.g. Harper, 1964; Hart et al., 1968; Berger & York, 1981). This will be resolved as more U-Pb data are collected from other parts of the Netoni Intrusive Complex and elsewhere in the Bird's Head Peninsula.

5.3 Metamorphic and deformation history

The granites and surrounding country rock have both undergone metamorphism and deformation. The country rocks have undergone at least two periods of deformation with development of a schistose fabric followed by extensional shearing (Fig. 4e), while the granites show only one period of deformation (partial recrystallisation of quartz/feldspar, development of quartz proto-ribbons etc.). It is likely that the country rocks had already undergone one period of deformation prior to granite intrusion.

The most intense deformation observed in both the granitoids and the country rocks appears to be isolated in small E-W striking mylonite bands. The age of these deformation phases is unknown. However, we suspect that these fabrics developed due to movement along the Sorong Fault Zone, as the fabrics share the same E-W orientation as the major fault zone. In terms of timing, all that we know is that the

deformation occurred after the crystallisation of the granites in the Triassic. This does not conflict with previous work as most workers propose that the Sorong Fault Zone is a relatively young feature (Cenozoic-Recent) (e.g. Hall, 2002).

The metamorphic country rocks show evidence of high-grade regional metamorphism (~500-600°C, 5 kbar) and there is also evidence of partial recrystallisation of quartz and feldspar in the granites at >400°C. The highest-grade metamorphic country rocks have myrmekite textures (a feature of higher temperature metamorphism; ~600°C – Phillips, 1980; Passchier & Trouw, 1996). These textures were not observed in any of the granite samples. We propose that the myrmekites reflect recrystallisation associated with the granite intrusions. We doubt the myrmekite reflects deformation associated with movement along the Sorong Fault Zone as we would then expect to see evidence for these textures in the granitoids as well as the metamorphic country rocks.

5.4 Tectonic evolution

The petrological, geochemical and geochronological data presented here indicate that the Netoni Intrusive Complex was emplaced during the Triassic, most likely in a continent-arc (Andean) type plate tectonic setting. This interpretation differs from some previous proposals for rift-related magmatism associated with a passive margin system during the Permo-Triassic (e.g. Pigram & Panggabean, 1984; Pigram & Davies, 1987; Pigram & Symonds, 1991), but is in agreement with other workers who have proposed that an Andean-type subduction zone occurred along the northern margin of the Australian continent at this time (Charlton, 2001; Hill & Hall, 2003; Gunawan et al., 2012; 2014).

Several other Carboniferous to Triassic granites are found in the Bird's Head, these include; the Melaiurna Granite (326 Ma, K-Ar), the Wajori Granite (295 Ma, K-Ar), the Wariki Granodiorite (258-226 Ma, K-Ar), the Anggi Granite (243-225 Ma, K-Ar) (all compiled in Bladon, 1988) and the Sorong Granite (224 ± 11 Ma, K-Ar) (Amri et al., 1990). We suspect that these granitoids could have been generated in the same Andean type continent margin as the Netoni Intrusive Complex but this requires new geochemical, petrographical and geochronological data. Farther east in Papua New Guinea, similar Triassic ages have been reported for tonalites from the Kubor Intrusive Complex (241.5 ± 3.2 Ma) (Van Wyck & Williams, 2002) and in the Amanab Metadiorite Complex (240 ± 3 Ma and 216 ± 3.2 Ma) (Crowhurst et al., 2004). Crowhurst et al. (2004) proposed that the older sample in the Amanab Metadiorite Complex formed as part of a Middle Triassic arc while the younger sample formed during Late Triassic extension. This interpretation, however was largely based on fitting the data to existing tectonic models (Pigram & Panggabean, 1984; Pigram & Davies, 1987; Pigram & Symonds, 1991) rather than isotopic or chemical data (which were not available at the time of their study). We found no clear petrological or geochemical distinction between Early, Middle, and Late Triassic Netoni granites, so we see no reason to invoke a change in tectonic regime to explain the petrogenesis of these granitoids.

Further support for a Permo-Triassic arc system along the length of New Guinea can be found in contemporaneous and younger sedimentary rocks. A detailed provenance study on the Tipuma Formation of the Bird's Head by Gunawan et al. (2012) revealed that the fluvial sandstones in this unit contain detrital volcanic quartz (showing melt

embayment features) and volcanic lithic fragments from an acidic Andean-type margin in the northern Bird's Head. Zircons from these sediments record Permo-Triassic ages with a median age of ~240 Ma (Gunawan et al., 2012). This correlates well with the U-Pb ages from the Netoni Intrusive Complex and the river sands presented here (248–213 Ma) (Fig. 12). The Netoni Intrusive Complex might therefore represent an intrusive equivalent of ash fall or acid volcanics that were deposited and later reworked and preserved within the Tipuma Formation (Fig. 12). Zircons of this age have also been reported from further afield in the Banda Arc (Zimmermann and Hall, 2016). So, the results reported here lend further support to a source of Triassic volcanic detritus being shed from New Guinea to the south over parts of what is now eastern Indonesia and north/northwestern Australia.

6. CONCLUSIONS

The Netoni Intrusive Complex represents a suite of deformed and partially recrystallised granite, granodiorite and rare pegmatite. These granitoids intruded previously metamorphosed medium to high-grade schist and gneiss, with melt injection occurring through dyke and sill networks. This caused contact metamorphism of the country rocks, which were also entrained as xenoliths and roof pendants within the Netoni granitoids. U-Pb zircon geochronology shows the granitoids crystallised at different points during the Early to Late Triassic (248–213 Ma). The geochemical data of these granitoids indicates that these have peraluminous, calc-alkalic to alkali-calcic and ferroan to magnesian compositions. The trace element geochemistry of these granites shows what is typically considered a subduction zone signature along with evidence for assimilation and fractional crystallisation with the surrounding country rock. These data support previous proposals that a continent-arc

subduction setting was active along the northern margin of the Australian plate (then part of eastern Gondwana) during the Permo-Triassic. The volcanic ejecta from this arc and its subsequent erosion were deposited in fluvial systems in the Bird's Head Peninsula and were potentially transported to parts of what is now eastern Indonesia and north/northwestern Australia.

ACKNOWLEDGEMENTS

We would like to thank the consortium of energy companies who funded this research as part of the Southeast Asia Research Group (ENI, Murphy Oil, Repsol, Shell, Engie, Statoil and Inpex). We would also thank Robert Hall and Mike Cottam for their advice on aspects of this work. Benjamin Jost, Indra Gunawan, Herwin Tiranda and Jumiko Sarira are thanked for their help in the field as well as for other logistical support. Robert Holm and another anonymous reviewer are thanked for their comments which led to a much improved manuscript. Christina Manning, Matthew Thirlwall and Martin Rittner are thanked for assistance collecting geochemical and isotopic data.

REFERENCES

Allen, C. M. & Campbell, I. H. 2012. Identification and elimination of a matrix-induced systematic error in LA-ICP-MS $^{206}Pb/^{238}U$ dating of zircon. Chemical Geology 332-333, 157-165.

Amri, C., Harahap, B. H., Pieters, P. E., & Bladon, G. M. 1990. Geology of the Sorong Sheet area, Irian Jaya, 1: 250.000 map and explanatory notes.

Audley-Charles, M. G. 1991. Tectonics of the New Guinea area. Earth and Planetary Sciences, Annual Review, 19, 17-41.

Audley-Charles, M. G., Ballantyne, P. D., & Hall, R. 1988. Mesozoic-Cenozoic rift-drift sequence of Asian fragments from Gondwanaland. Tectonophysics, 155(1), 317-330.

Bailly, V., Pubellier, M., Ringenbach, J. C., De Sigoyer, J., & Sapin, F. 2009. Deformation zone 'jumps' in a young convergent setting; the Lengguru fold-and-thrust belt, New Guinea Island. Lithos, 113(1), 306-317.

Berger, G. W., & York, D. 1981. Geothermometry from 40Ar39Ar dating experiments. Geochimica et Cosmochimica Acta, 45(6), 795-811.

Black, L. P., Kamo, S. L., Allen, C. M., Davis, D. W., Aleinikoff, J. N., Valley, J. W., Mundil, R., Campbell, I. H., Korsch, R. J., Williams, I. S., Foudoulis, C. 2004. Improved $^{206}Pb/^{238}U$ microprobe geochronology by the monitoring of a trace-element-related matrix effect; SHRIMP, ID–TIMS, ELA–ICP–MS and oxygen isotope documentation for a series of zircon standards. Chemical Geology, 205(1–2), 115-140.

Bladon, G. M. 1988. Preliminary geological report. Catalogue, appraisal and significance of K-Ar isotopic ages determined for igneous and metamorphic rocks in Irian Jaya. Indonesia-Australia Geological Mapping Project, 79pp.

Brown, G. C., Thorpe, R. S., & Webb, P. C. 1984. The geochemical characteristics of granitoids in contrasting arcs and comments on magma sources. Journal of the Geological Society, 141(3), 413-426.

Charlton, T. R. 1996. Correlation of the Salawati and Tomori Basins, eastern Indonesia: a constraint on left-lateral displacements of the Sorong fault zone. Geological Society, London, Special Publications, 106(1), 465-481.

Charlton, T. R. 2001. Permo-Triassic evolution of Gondwanan eastern Indonesia, and the final Mesozoic separation of SE Asia from Australia. Journal of Asian Earth Sciences, 19(5), 595-617.

Chevallier, B., & Bordenave, M. L. 1986. Contribution of geochemistry to the exploration in the Bintuni Basin, Irian Jaya. Paper presented at the Indonesian Petroleum Association, Proceedings 15th Annual Convention, Jakarta.

Crowhurst, P. V., Maas, R., Hill, K. C., Foster, D. A., & Fanning, C. M. 2004. Isotopic constraints on crustal architecture and Permo - Triassic tectonics in New Guinea: Possible links with eastern Australia. Australian Journal of Earth Sciences, 51(1), 107-124.

Dow, D. B., & Sukamto, R. 1984. Western Irian Jaya: the end-product of oblique plate convergence in the late Tertiary. Tectonophysics, 106(1), 109-139.

Dow, D. B., Robinson, G. P., Hartono, U., & Ratman, N. 1988. Geology of Irian Jaya: Preliminary Geological Report. Geological Research and Development Centre - Bureau of Mineral Resources, Canberra.

Frost, B. R., Barnes, C. G., Collins, W. J., Arculus, R. J., Ellis, D. J., & Frost, C. D. . 2001. A geochemical classification for granitic rocks. Journal of Petrology, 42(11), 2033-2048.

Gale, A., Dalton, C. A., Langmuir, C. H., Su, Y., & Schilling, J. G. 2013. The mean composition of ocean ridge basalts. Geochemistry, Geophysics, Geosystems, 14(3), 489-518.

Giddings, J. W., Sunata, W., & Pigram, C. 1993. Reinterpretation of palaeomagnetic results from the Bird's Head, Irian Jaya: new constraints on the drift history of the Kemum Terrane. Exploration Geophysics, 24(2), 283-290.

Gunawan, I. 2012. Age, Character and provenance of the Tipuma Formation, West Papua: New insights from detrital zircon dating. Paper presented at the Indonesian Petroleum Association, Proceedings 36th Annual Convention, Jakarta.

Gunawan, I., Hall, R., & Sapiie, B. 2014. Triassic Reservoir Characteristics of the Bird's Head, New Guinea, Indonesia: New Insights from Provenance Study. International Petroleum Technology Conference.

Hall, R. 2002. Cenozoic geological and plate tectonic evolution of SE Asia and the SW Pacific: computer-based reconstructions, model and animations. Journal of Asian Earth Sciences, 20(4), 353-434.

Hall, R. 2012. Late Jurassic-Cenozoic reconstructions of the Indonesian region and the Indian Ocean. Tectonophysics 570-571, 1-41.

Hamilton, W. B. 1979. Tectonics of the Indonesian region (No. 1078). US Govt. Print. Off.

Harper, C. T. 1964. Potassium-argon ages of slates and their geological significance. Nature, 203, 468-470.

Hart, S. R., Davis, G. L., Steiger, R. H., & Tilton, G. R. 1968. A comparison of the isotopic mineral age variations and petrologic changes induced by contact metamorphism. Radiometric dating for geologists, 73-110.

Harris, N. B., Pearce, J. A., & Tindle, A. G. 1986. Geochemical characteristics of collision-zone magmatism. Geological Society, London, Special Publications, 19(1), 67-81.

Hawkesworth, C. J., Hammill, M., Gledhill, A. R., van Calsteren, P., & Rogers, G. 1982. Isotope and trace element evidence for late-stage intra-crustal melting in the High Andes. Earth and Planetary Science Letters, 58(2), 240-254.

Hill, K. C., & Hall, R. 2003. Mesozoic-Cenozoic evolution of Australia's New Guinea margin in a west Pacific context. Geological Society of Australia Special Publication 22 and Geological Society of America Special Paper 372, 265-289.

Jackson, S. E., Pearson, N. J., Griffin, W. L., & Belousova, E. A. 2004. The application of laser ablation-inductively coupled plasma-mass spectrometry to in situ U–Pb zircon geochronology. Chemical Geology, 211(1–2), 47-69.

Jochum, K. P., Weis, U., Stoll, B., Kuzmin, D., Yang, Q., Raczek, I., Jacob, D. E., Stracke, A. Birbaum, K., Frick, D. A., Gunther, D., Enzweiler, J. 2011. Determination of Reference Values for NIST SRM 610–617 Glasses Following ISO Guidelines. Geostandards and Geoanalytical Research, 35(4), 397-429.

Ludwig, K. R. 2009. Isoplot 4.1. A Geochronological Toolkit for Microsoft Excel. Berkeley Geochronology Center, Berkeley.

McDougall, I. 1962. Differentiation of the Tasmanian dolerites: Red Hill dolerite-granophyre association. Geological Society of America Bulletin, 73(3), 279-316.

Metcalfe, I. 1990. Allochthonous terrane processes in Southeast Asia. Philosophical Transactions Royal Society of London, A331, 625-640.

Metcalfe, I. 1998. Palaeozoic and Mesozoic geological evolution of the SE Asian region: multidisciplinary constraints and implications for biogeography. In Hall, R. & Holloway, J. D. (eds.) Biogeography and Geological Evolution of SE Asia. Backhuys Publishers, Leiden, The Netherlands, 25-41.

Middlemost, E. A. 1994. Naming materials in the magma/igneous rock system. Earth-Science Reviews, 37(3), 215-224.

Miyashiro, A. 1970. Volcanic rock series in island arcs and active continental margins. American journal of science, 274(321-355).

Palme, H., & O'Neill, H. S. C. 2003. Cosmochemical estimates of mantle composition. Treatise on geochemistry, 2, 1-38.

Passchier, C. W., & Trouw, R. A. 1996. Microtectonics Berlin: Springer.

Paton, C., Woodhead, J. D., Hellstrom, J. C., Hergt, J. M., Greig, A., & Maas, R. 2010. Improved laser ablation U- Pb zircon geochronology through robust downhole fractionation correction. Geochemistry, Geophysics, Geosystems, 11(3).

Paton, C., Hellstrom, J., Paul, B., Woodhead, J., & Hergt, J. 2011. Iolite: Freeware for the visualisation and processing of mass spectrometric data. Journal of Analytical Atomic Spectrometry, 26(12), 2508-2518.

Pearce, J. 1996. Sources and settings of granitic rocks. Episodes, 19, 120-125.

Pearce, J. A., Harris, N. B., & Tindle, A. G. 1984. Trace element discrimination diagrams for the tectonic interpretation of granitic rocks. Journal of petrology, 25(4), 956-983.

Petrus, J. A., & Kamber, B. S. 2012. VizualAge: A Novel Approach to Laser Ablation ICP- MS U- Pb Geochronology Data Reduction. Geostandards and Geoanalytical Research, 36(3), 247-270.

Perkins, T. W., & Livsey, A. R. 1993. Geology of the Jurassic gas discoveries in Bintuni Bay, western Irian Jaya. Paper presented at the Indonesian Petroleum Association, Proceedings 22nd Annual Convention, Jakarta.

Phillips, E. R. 1980. On polygenetic myrmekite. Geological Magazine, 117(01), 29-36.

Phoa, R. S., & Samuel, L. 1986. Problems of source rock identification in the Salawati Basin, Irian Jaya. Paper presented at the Indonesian Petroleum Association, Proceedings 15th Annual Convention, Jakarta.

Pieters, P. E., Hartono, U., & Amri, C. 1989. Geologi lembar Mar, Irian Jaya. Geological Survey of Indonesia, Directorate of Mineral Resources, Geological Research and Development Centre, Bandung, 62pp.

Pieters, P. E., Pigram, C. J., Trail, D. S., Dow, D. B., Ratman, N., & Sukamto, R. 1983. The stratigraphy of western Irian Jaya. Indonesian Petroleum Association, Proceedings 12th annual convention, Jakarta, 1983, I, 229-262.

Pieters, P. E., Ryburn, R. J., & Trail, D. S. 1979. Geological reconnaissance in Irian Jaya, 1976 and 1977. Geological Research and Development Centre, Indonesia, unpublished report, 19.

Pigram, C. T., & Davies, H. L. 1987. Terranes and the accretion history of the New Guinea orogen. BMR Journal of Australian Geology and Geophysics, 10, 193-211.

Pigram, C. and Symonds, P. A. 1991. A review of the timing of the major tectonic events in the New Guinea Orogen. Journal of Southeast Asian Earth Sciences 6, 307-318.

Pigram, C. J., & Panggabean, H. 1984. Rifting of the northern margin of the Australian continent and the origin of some microcontinents in eastern Indonesia. Tectonophysics, 107(3-4), 331-353.

Pryer, L. L. 1993. Microstructures in feldspars from a major crustal thrust zone: the Grenville Front, Ontario, Canada. Journal of Structural Geology, 15(1), 21-36.

Reed, W. P. 1992. Certificate of Analysis: Standard Reference Materials 610 and 611. National Institute of Standards and Technology.

Rudnick, R. L., & Gao, R. 2003. Composition of the continental crust, treatise of geochemistry, vol. 3.

Sambridge, M. S., & Compston, W. 1994. Mixture modeling of multi-component data sets with application to ion-probe zircon ages. Earth and Planetary Science Letters, 128(3-4), 373-390.

Shand, S. J. 1943. Eruptive rocks: their genesis, composition, and classification, with a chapter on meteorites: J. Wiley & sons, inc.

Sláma, J., Košler, J., Condon, D. J., Crowley, J. L., Gerdes, A., Hanchar, J. M., Horstwood, M. S. A., Morris, G. A., Nasdala, L., Norberg, N., Schaltegger, U., Schoene, B., Tubrett, M. N., Whitehouse, M. J. 2008. Plešovice zircon — A new natural reference material for U–Pb and Hf isotopic microanalysis. Chemical Geology, 249(1–2), 1-35.

Struckmeyer, H. I. M., Yeung, M., & Pigram, C. J. 1993. Mesozoic to Cainozoic plate tectonic and palaeogeographic evolution of the New Guinea region. In Petroleum Exploration and Development in Papua New Guinea, Port Moresby. Proceedings of 2nd PNG Petroleum Convention, pp. 261-290.

Tera, F., & Wasserburg, G. J. 1972. U-Th-Pb systematics in three Apollo 14 basalts and the problem of initial Pb in lunar rocks. Earth and Planetary Science Letters, 14(3), 281-304.

Thorpe, R. S., Francis, P. W., O'Callaghan, L., Hutchison, R., & Turner, J. S. 1984. Relative Roles of Source Composition, Fractional Crystallization and Crustal Contamination in the Petrogenesis of Andean Volcanic Rocks [and Discussion]. Philosophical Transactions of the Royal Society of London A: Mathematical, Physical and Engineering Sciences, 310(1514), 675-692.

Trouw, R. A., Passchier, C. W., & Siersma, D. 2009. Atlas of Mylonites-and related microstructures. Springer Science & Business Media.

Van Wyck, N. and Williams, I. S. 2002. Age and provenance of basement metasediments from the Kubor and Bena Bena Blocks, central Highlands, Papua New Guinea: constraints on the tectonic evolution of the northern Australian cratonic margin. Australian Journal of Earth Sciences 49, 565-577.

Vernon, R. H. 2004. A Practical Guide to Rock Microstructure. Cambridge University Press.

Visser, W. A., & Hermes, J. J. 1962. Geological results of the exploration for oil in Netherlands New Guinea: carried out by the Nederlandsche Nieuw Guinee Petroleum Maatschappij 1935-1960. Staatsdrukkerij-en Uitgeverijbedrijf.

White, L. T. & Ireland, T. R. 2012. High-uranium matrix effect in zircon and its implications for SHRIMP U-Pb age determinations. Chemical Geology 306-307, 78-91.

White, L. T., Ahmad, T., Ireland, T. R., Lister, G. S., & Forster, M. A. 2011. Deconvolving episodic age spectra from zircons of the Ladakh Batholith, northwest Indian Himalaya. Chemical Geology 289, 179-196.

Wilson, M. 1989. Igneous petrogenesis: A global tectonic approach. London: Unwyn Hyman.

Zen, E. A. 1986. Aluminum enrichment in silicate melts by fractional crystallization: some mineralogic and petrographic constraints. Journal of Petrology, 27(5), 1095-1117.

Zimmermann, S. and Hall, R. 2016. Provenance of Triassic and Jurassic sandstones in the Banda Arc: Petrography, heavy minerals and zircon geochronology. Gondwana Research, 37, 1-19.

Figure Captions

Figure 1. Location and simplified geological maps of the Bird's Head Peninsula. (a) Present-day location of the Bird's Head and New Guinea, with current plate tectonic boundaries. Modified from Hill and Hall (2003). (b) Simplified geological map of the Bird's Head displaying the dominant lithologies and fault zone in the region, as well as the location of the study area. Location and extent of dominant lithologies and fault zones are adapted from Pieters et al. (1989).

Figure 2. Detailed geological map, displaying the lithostratigraphic units found in the study area. This map focuses on the Netoni Intrusive Complex and the main trace of the Sorong Fault Zone. It also shows the GPS tracks of the traverses, the location of each sample taken and the position of roads and villages. (a) Detail of river traverse 1. (b) Detail of river traverse 2. Location and extent of geological units and fault zone are from Pieters et al. (1989).

Figure 3. Photographs of metasedimentary country rocks in the Netoni Intrusive Complex. (a) Amphibolite/granite contact displaying the intrusion of small granite dykes into amphibolite. (b) Gneissic banding separating layers of leucocratic quartzo-feldspathic material from melanocratic ferromagnesian mineral rich layers (lens cap 3cm across). (c) Pegmatite veins in biotite-gneiss, showing pinch and swell structures and offsets by later extensional faulting (shown in white). (d) Hand specimen of granodiorite sill in mica schist host rock. Quartz aggregates within the dyke display asymmetrical boudins and quartz ribbons are present in the mica schist.

Figure 4. Photomicrographs of mineralogical and textural features in metasedimentary country rocks from the Netoni Intrusive Complex (Figure 4a, 4c and 4f in plane polarised light – Figure 4b, 4d and 4e in cross-polarised light). (a) Embayed hypidioblastic garnet porphyroblast within quartzo-feldspathic leucosome. (b) Sillimanite porphyroblasts within biotite-rich melanosome. (c) Boundary between biotite-rich lenses and hornblende-rich material. (d) Late, quartz filled normal shear zones offsetting quartzo-feldspathic aggregates. (e) Weakly developed C' shear bands displaying normal sense of shear. (f) High temperature bulbous myrmekite.

Figure 5. Photographs of granite-country rock and intrusive relationships in the Netoni Intrusive Complex. (a) Muscovite-rich pegmatite vein within granite. (b) Granite dyke cross-cutting country rock foliation. (c) Granite sill or stock intruded parallel to country rock foliation with partially melted country rock xenoliths entrained within the granite. (d) Chaotic intrusion and veining of granite (light in colour) in metamorphic country rock (dark in colour), granite melt has isolated and fragmented the once coherent country rock. (e) Intrusion of leucocratic granite sills along quartz-biotite schist foliation planes (lens cap is 3cm across). (f) Large roof pendant of country rock xenolith within granite.

Figure 6. Photomicrographs displaying mineralogy and brittle/ductile deformation within granites of the Netoni Intrusive Complex. (a) Presence of muscovite in granite from the Netoni Intrusive Complex (MW14-09). (b) Extensional shear sense on broken feldspar within cataclasite (MW14-02). (c) Dynamic recrystallisation of quartz with subgrain rotation (SGR) and bulging recrystallisation (BLG) defining a fabric (MW14-17). (d) Dynamic recrystallisation of quartz in MW14-07 with SGR, BLG

and quartz proto-ribbons defining the fabric. (e) Recrystallised feldspar between two larger feldspars, MW14-02. (f) Kinking of plagioclase crystal and replacement of biotite by chlorite in MW14-03.

Figure 7. Major element discrimination diagrams for granites from the Netoni Intrusive Complex. (a) Total alkalis vs silica diagram (TAS) (Middlemost, 1994) for granites of the Netoni Intrusive Complex. (b) Plot of Netoni granites according to their MALI vs SiO_2 concentrations. Data fields proposed by Frost et al. (2001). (c) Fe Index vs SiO_2 plot for the Netoni granites using the fields proposed by Frost et al. (2001). (d) A/NK vs ASI plot of the Netoni granites using the classification proposed by Shand (1943).

Figure 8. Multiple trace element plots for granites from the Netoni Intrusive Complex normalised to (a) continental crust values (Rudnick & Gao, 2003) (b) primitive mantle values (Palme & O'Neill, 2003) and (c) ALL MORB values (Gale et al., 2013).

Figure 9. Tera-Wasserburg concordia plots with 2σ error ellipses for the five granite samples from the Netoni Intrusive Complex and the two river sand samples. Analyses that are ±10% discordant have been omitted (cf. Supplementary Data File 2 for further details).

Figure 10. Weighted mean age plots of U-Pb zircon ages from all granite samples analysed from the Netoni Intrusive Complex. Errors represent 95% confidence.

Figure 11. Probability density plots showing all concordant zircon ages obtained from the sands of two rivers that sample the Netoni Intrusive Complex. All U-Pb ages displayed with 2σ errors.

Figure 12. Probability density plots showing the combined U-Pb zircon ages for (a) all granite samples from the Netoni Intrusive Complex, (b) the two river sands, and (c) the Tipuma Formation (data from Gunawan et al., 2012 – showing a subset of the dataset between 150 Ma and 350 Ma).

Figure 13. Proposed tectonic setting of the Bird's Head at ~240 Ma. The northeastern margin of the Bird's Head at that time is the location of an Andean-type continental volcanic margin with SW subduction of the Palaeo-Pacific Plate beneath the Australian Plate producing acidic volcanism. The coeval Netoni Intrusive Complex (as well as other local Permo-Triassic granitoids) feed this volcanism, zircons from which are in turn deposited as eroded detritus or volcanic ejecta in the local Tipuma Formation and possibly further afield.

Table Captions

Table 1. All granitic and river sand samples analysed from the Netoni Intrusive Complex (mineral abbreviations – Qz; quartz, Pl: plagioclase, Kfs: K-feldspar, Bt: biotite, Ms: Muscovite, Acc: accessory minerals).

Table 2. XRF major and trace element data for all granite samples from the Netoni Intrusive Complex. Analyses with an * are below the limit of detection (LoD).

Table 3. U-Pb ages of the Netoni Intrusive Complex presented here, compared with K-Ar age data from the literature (Bladon 1988).

Supplementary Data

Supplementary File 1: Configuration and parameters of the LA-ICPMS used at UCL for U-Pb analyses on zircon separates for each sample.

Supplementary File 2: U-Pb and trace element values for LA-ICP-MS analyses on zircons for all samples that were analysed as part of this study.

Supplementary File 3: Scanning electron microscope cathodoluminescence images of zircon grains from all granite and river sand samples from the Netoni Intrusive Complex, along with laser spot locations and analyses numbers.

Sample	Latitude	Longitude	Lithology	Texture	Mineralogy	Analyses
MW14-02	0°49'3.81"S	133° 6'28.45"E	(Syeno-) Granite	Porphyritic (Kfs phenocrysts), medium grained matrix	**Qz** (40%), **Kfs** (40%), **Pl** (15%), **Acc** (5%)	XRF, LA-ICP-MS
MW14-03	0°46'37.73"S	133° 2'27.26"E	(Syeno-) Granite	Equigranular, medium grained	**Qz** (20%), **Kfs** (55%), **Pl** (20%), **Bt** (5%)	XRF, LA-ICP-MS
MW14-04	0°46'37.73"S	133° 2'27.26"E	Granodiorite	Equigranular, medium grained	**Qz** (45%), **Pl** (30%), **Kfs** (10%), **Bt** (10%), **Acc** (5%)	-
MW14-05	0°46'37.73"S	133° 2'27.26"E	River Sand	-	-	LA-ICP-MS
MW14-07	0°46'39.15"S	133° 2'25.74"E	(Syeno-) Granite	Equigranular, medium grained	**Qz** (40%), **Kfs** (35%), **Pl** (15%), **Bt** (5%), **Acc** (5%)	XRF
MW14-08	0°46'39.15"S	133° 2'25.74"E	(Monzo-) Granite	Equigranular, medium grained	**Qz** (30%), **Kfs** (30%), **Pl** (30%), **Bt** (5%), **Acc** (5%)	XRF
MW14-09	0°46'40.65"S	133° 2'25.53"E	(Monzo-) Granite	Equigranular, medium grained	**Qz** (50%), **Kfs** (20%), **Pl** (20%), **Ms** (5%), **Bt** (5%)	LA-ICP-MS
MW14-11	0°46'47.85"S	133° 2'26.89"E	(Syeno-) Granite	Equigranular, medium grained	**Qz** (40%), **Kfs** (45%), **Pl** (10%), **Bt** (5%)	XRF, LA-ICP-MS
MW14-13	0°47'55.81"S	133°18'1.84"E	(Monzo-) Granite	Equigranular, medium grained	**Qz** (30%), **Kfs** (40%), **Pl** (25%), **Acc** (5%)	XRF
MW14-14	0°47’34.06”S	133°20’53.29”E	River Sand	-	-	LA-ICP-MS
MW14-17	0°47'34.06"S	133°20'53.29"E	(Syeno-) Granite	Equigranular, medium grained	**Qz** (30%), **Kfs** (50%), **Pl** (10%), **Bt** (10%)	XRF, LA-ICP-MS

Sample	MW14-02	MW14-03	MW14-07	MW14-08	MW14-11	MW14-13	MW14-17
Lithology	Granite	Granite	Granite	Granite	Granite	Granite	Granite
Major elements (wt.%)							
SiO_2	74.65	72.49	75.87	78.20	72.64	75.73	77.02
Al_2O_3	13.22	13.62	13.60	13.02	15.32	13.84	12.52
Fe_2O_3	1.90	2.65	0.69	0.15*	0.82	0.37*	1.39
MgO	0.07*	0.50	0.08*	0.06*	0.20	0.12*	0.15*
CaO	0.61	1.52	0.65	0.46	1.59	0.59	0.58
Na_2O	3.86	3.48	3.08	2.76	3.03	2.95	2.39
K_2O	4.96	4.39	5.52	4.96	6.14	6.47	5.98
TiO_2	0.23	0.33	0.05	0.03	0.09	0.05	0.10
MnO	0.07	0.05	0.01	0.00*	0.02	0.01	0.03
P_2O_5	0.04	0.08	0.02	0.03	0.05	0.03	0.03
SO_3	0.02	0.01	0.02	0.02	0.02	0.01	0.02
LOI	1.06	0.77	0.74	0.74	1.24	0.94	1.10
Major Total	99.63	99.12	99.58	99.70	99.93	100.17	100.21
Trace elements (ppm)							
Ni	2.3*	2.8*	2.6*	2.7*	2.6*	9.1	2.2*
Co	-0.9*	2.8*	5.3	1.8*	-2.4*	5.5	-4.1*
Cr	4.3*	3.8*	2.8*	3.8*	3.5*	5.4*	2.7*
V	6.9*	16.5	2.8*	3.7*	3.8*	7.0*	8.6
Sc	6.2	2.4*	2.9	-0.5*	3.0	0.1*	0.8*
Cu	2.5	3.0	4.8	2.4	3.2	3.6	2.3
Zn	51.6	44.2	4.7	1.1*	11.3	25.6	15.3
As	0.7	0.8	2.4	1.1	0.3	1.2	0.9
S	27	31	9	15	5	785	34
F	1041	298	115	144	90	106	108
Cl	125	88	68	64	60	71	59
Br	0.6	0.5	0.5	0.5	0.4	0.7	0.4
Ga	18.1	17.3	15.3	10.3	13.8	10.8	11.5
Pb	21.6	18.7	43.4	28.4	47.8	35.4	14.3
Sr	80.9	154.8	58.2	182.0	195.3	128.8	167.0
Rb	157.3	126.6	202.0	120.8	174.1	120.3	132.0
Ba	320.4	797.1	80.7	700.7	708.6	365.4	520.5
Zr	267.8	180.7	47.8	50.8	166.3	12.8	91.4
Nb	27.4	14.4	13.4	0.7*	8.2	1.0	3.7
Ta	2.3*	0.8*	1.0*	0.4*	1.4*	0.8*	1.0*
Mo	0.6	-0.1*	-0.2*	0.0*	0.2*	-0.5*	0.1*
Th	25.0	13.0	23.4	2.8	135.8	1.8	8.2
U	4.1	2.4	5.3	1.6	8.4	4.7	1.8
Y	48.9	24.6	39.7	8.4	37.9	11.1	5.5
La	95.2	39.5	8.0	5.4	81.0	2.3*	18.0
Ce	189.6	79.5	19.7	13.3	167.6	7.6	33.0
Nd	70.2	27.8	9.2	4.0*	66.2	3.9*	10.5
Sm	15.0	5.4*	4.2*	2.0*	13.3	2.1*	3.0*
Yb	5.0	2.7	3.4	1.1	2.7	1.4	1.0*
Hf	6.3	3.8	2.0	1.5	4.2	0.4	2.7
Cs	1*	-1*	0*	1*	1*	3	0*
Trace Element Total	0.29	0.23	0.09	0.15	0.23	0.11	0.14
Sum Total	99.92	99.34	99.67	99.85	100.16	100.28	100.35

Netoni Intrusive Complex

	U-Pb ages (This study)	**K-Ar ages (Bladon, 1988)**
Triassic	249.0 ± 3.5 Ma (Zircon)	241 Ma (Hornblende)
	241.1 ± 4.1 Ma (Zircon)	238 Ma (Hornblende)
	229.5 ± 4.1 Ma (Zircon)	230 Ma (Hornblende)
	227.2 ± 3.4 Ma (Zircon)	229 Ma (Hornblende)
	211.7 ± 2.9 Ma (Zircon)	225 Ma (Hornblende)
		208 Ma (Hornblende)
Jurassic		198 Ma (Biotite)
		174 Ma (Biotite)
		158 Ma (Hornblende)
Cretaceous		130 Ma (Plagioclase)
		84.1 Ma (Biotite)
		78.5 Ma (Plagioclase)
Neogene		6.7 Ma (Hornblende)

Figure 1

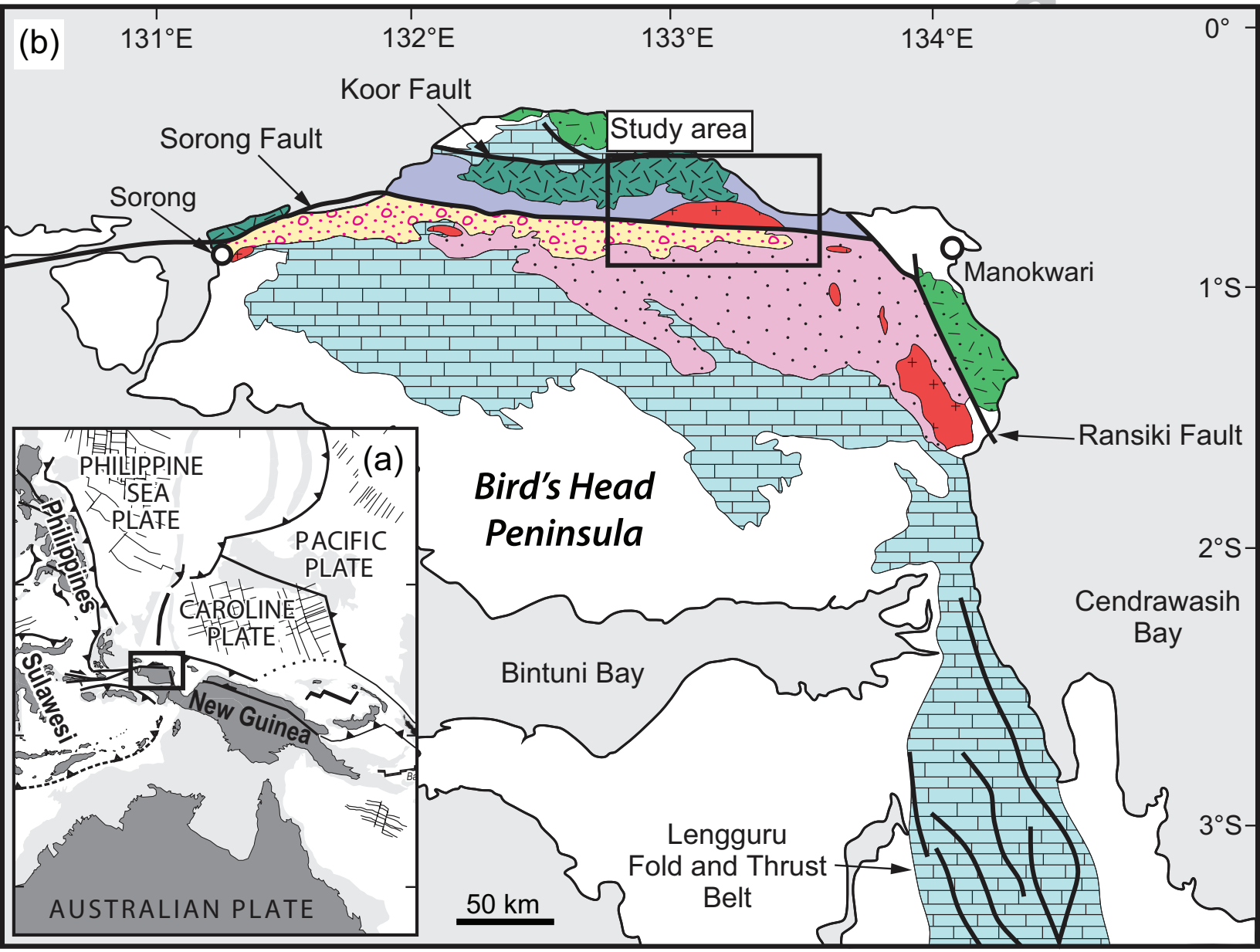

Figure 2

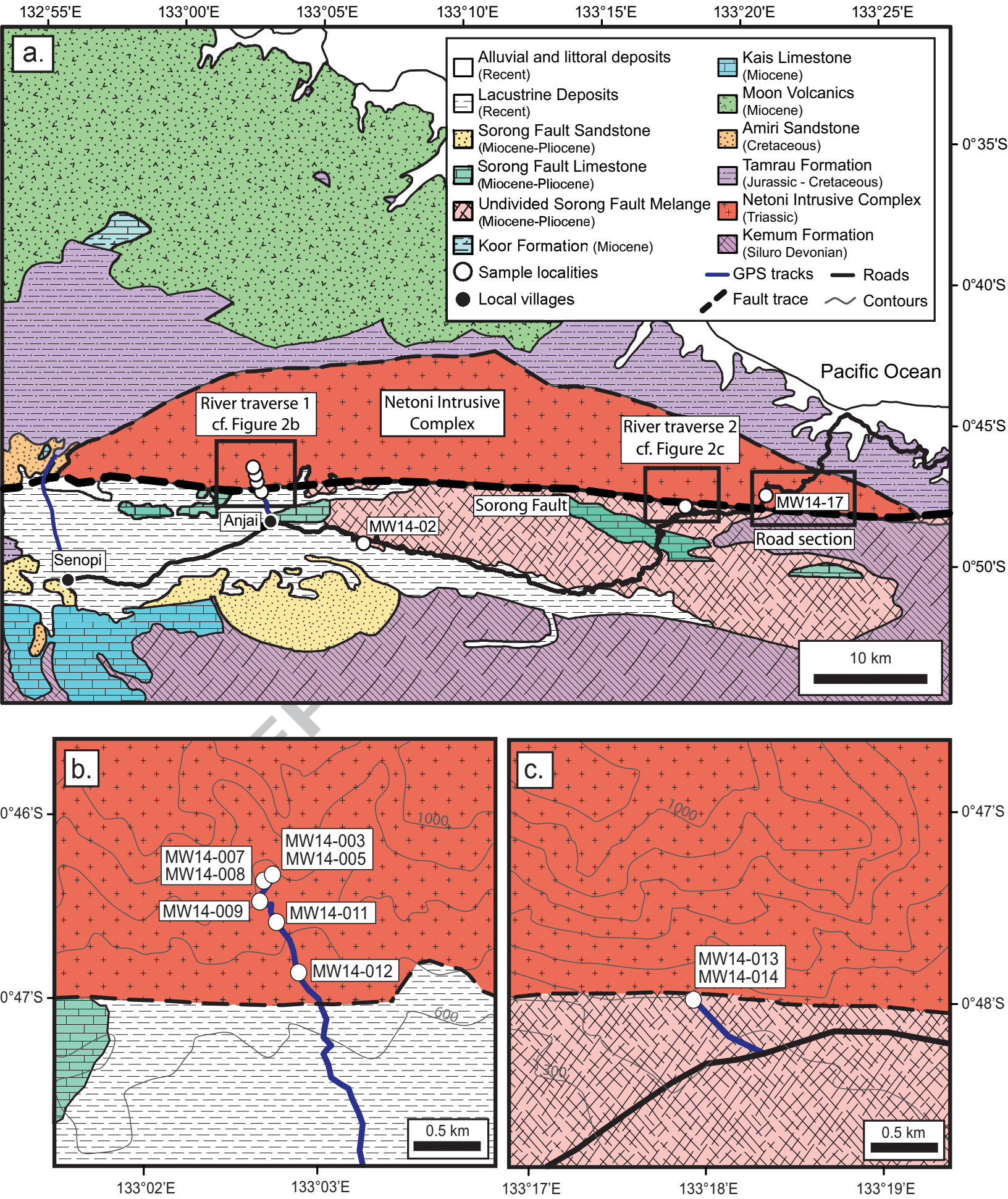

Figure 3

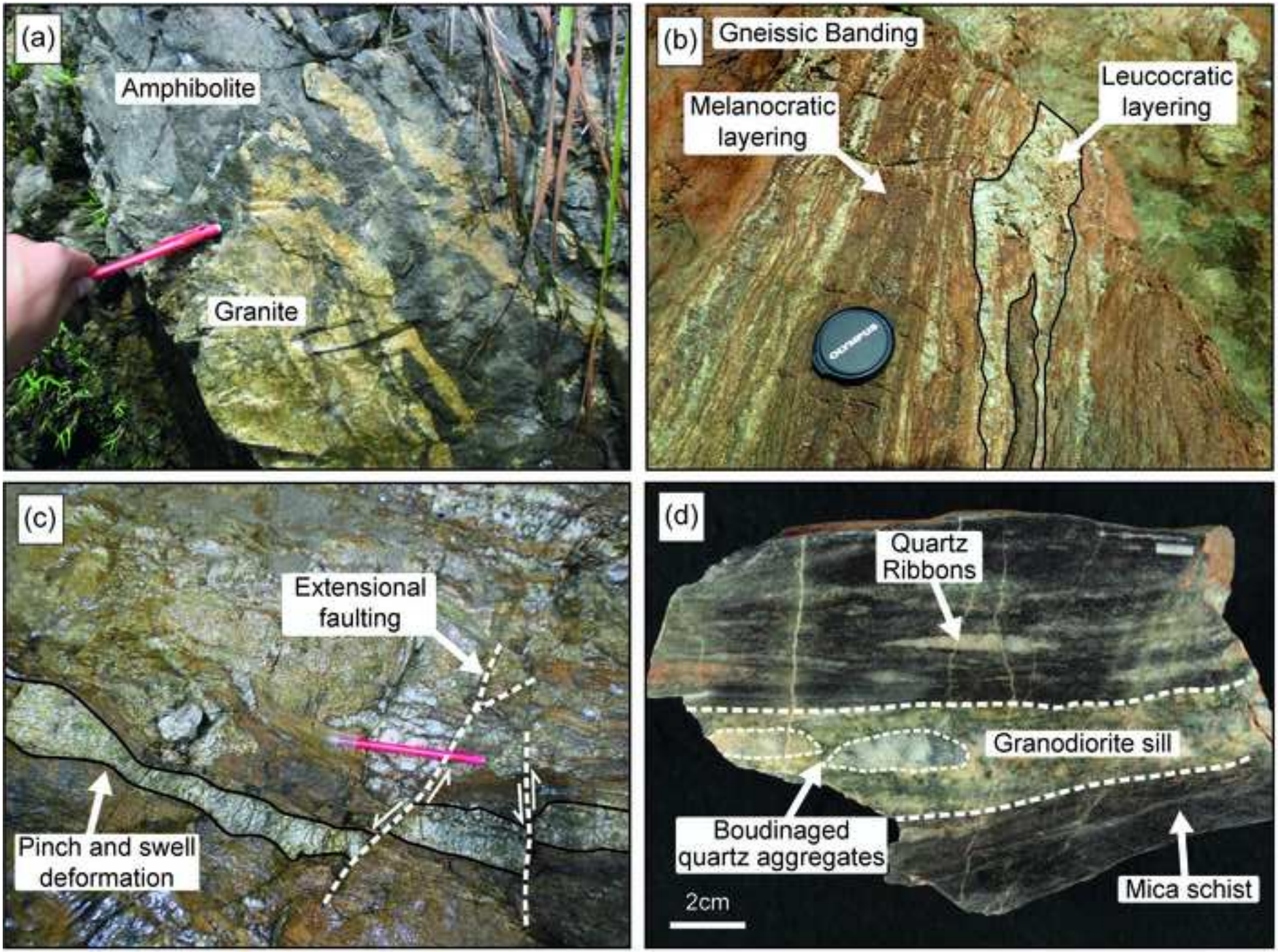

Figure 4

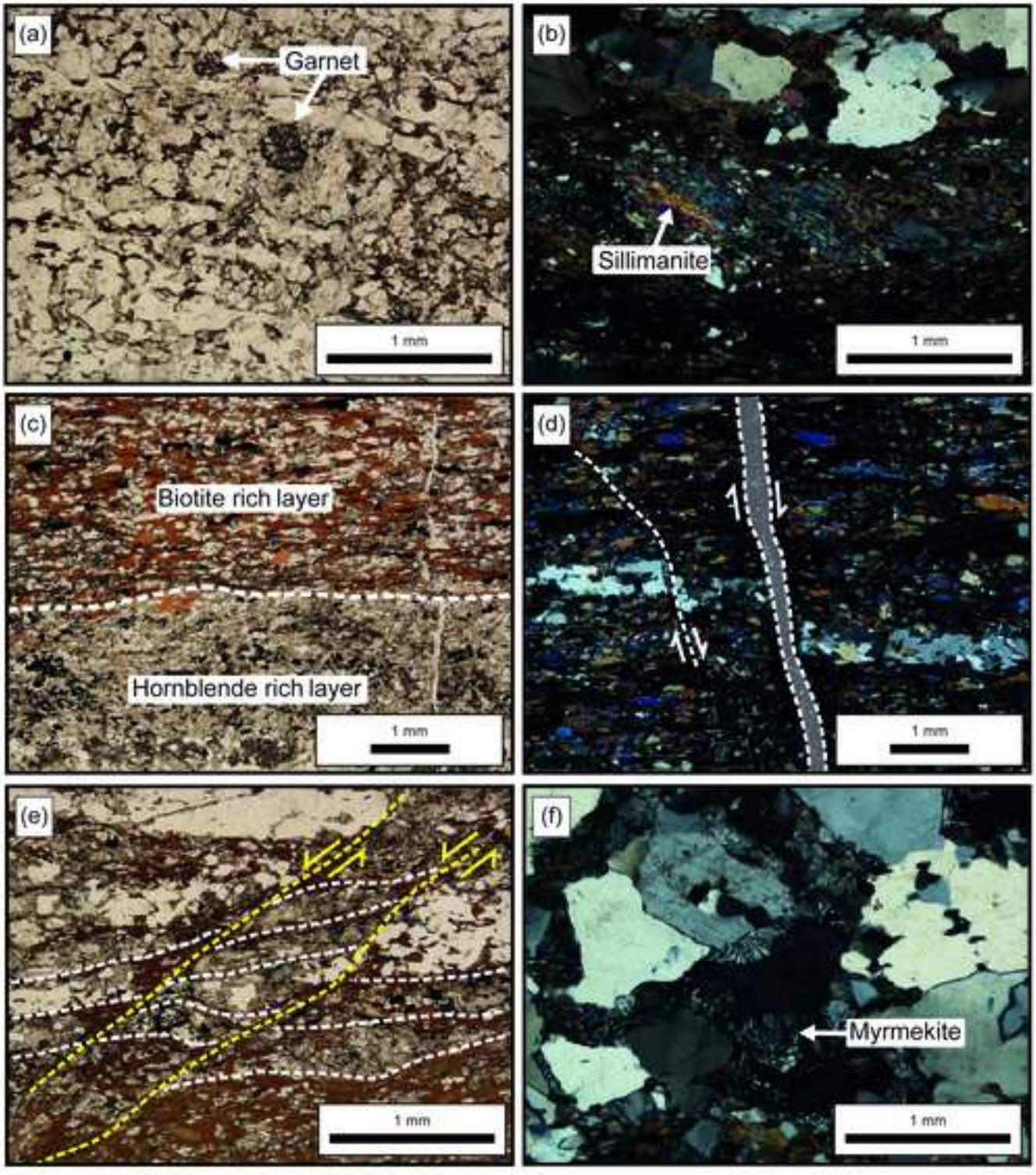

Figure 5

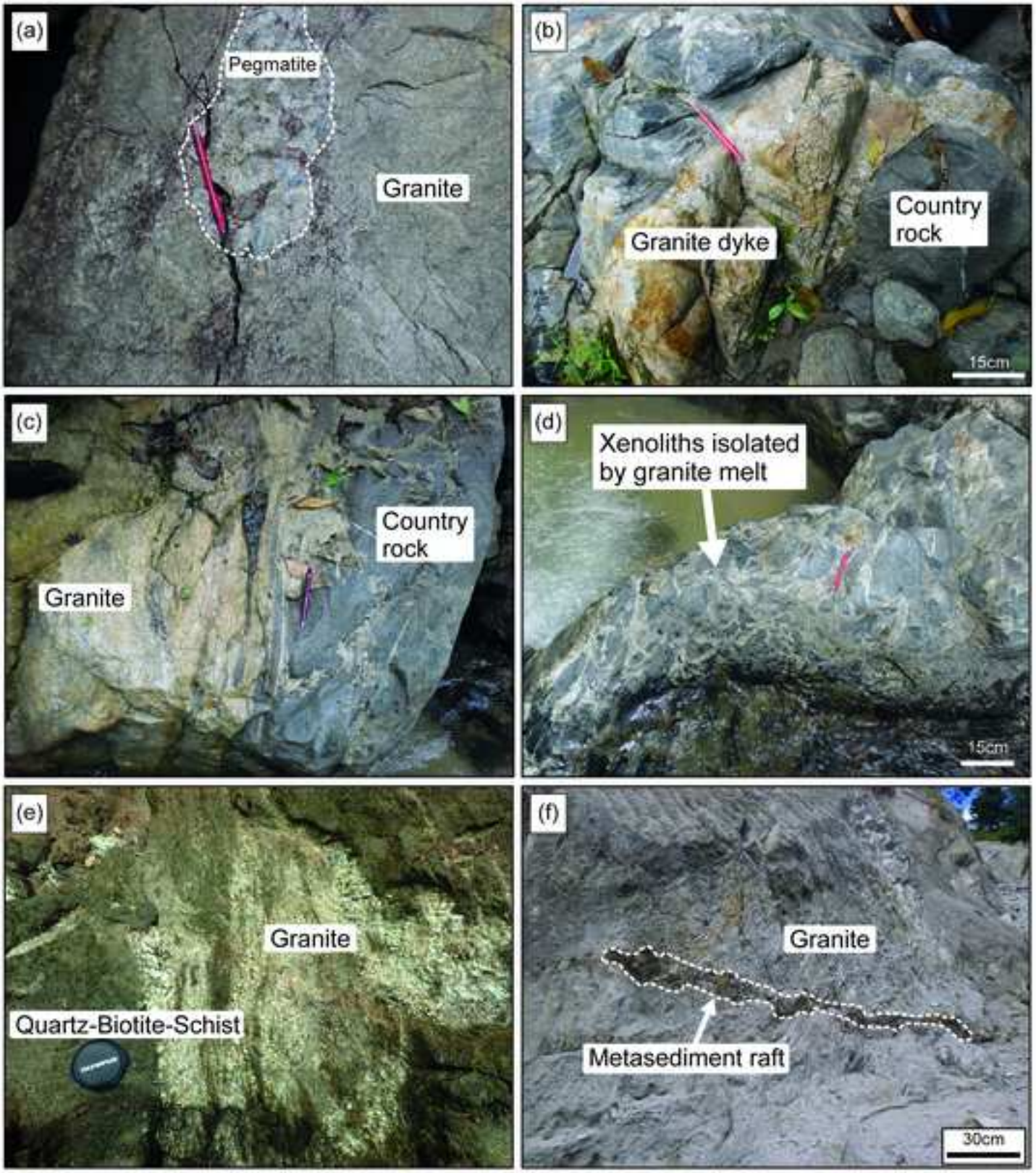

Figure 6

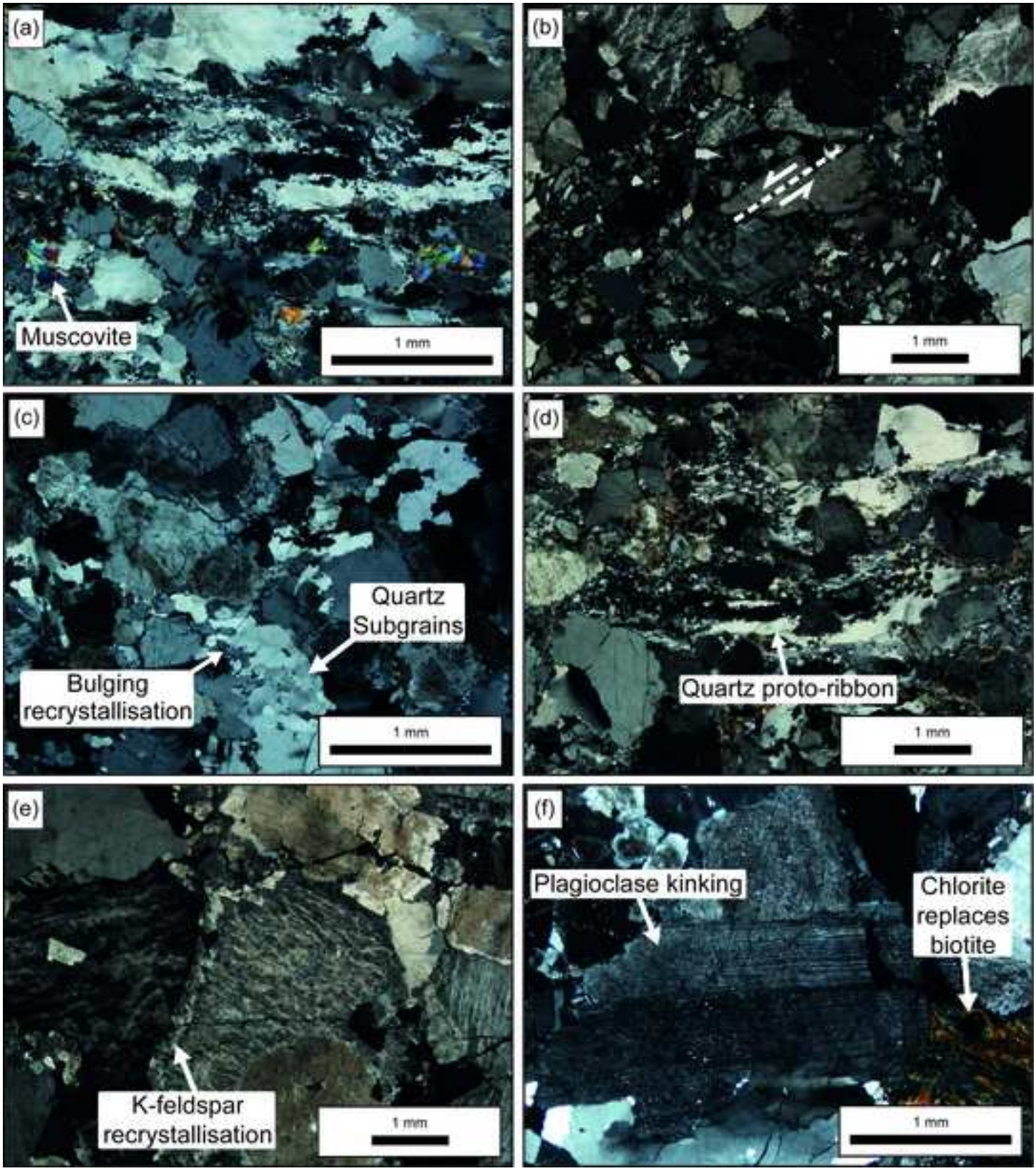

Figure 7

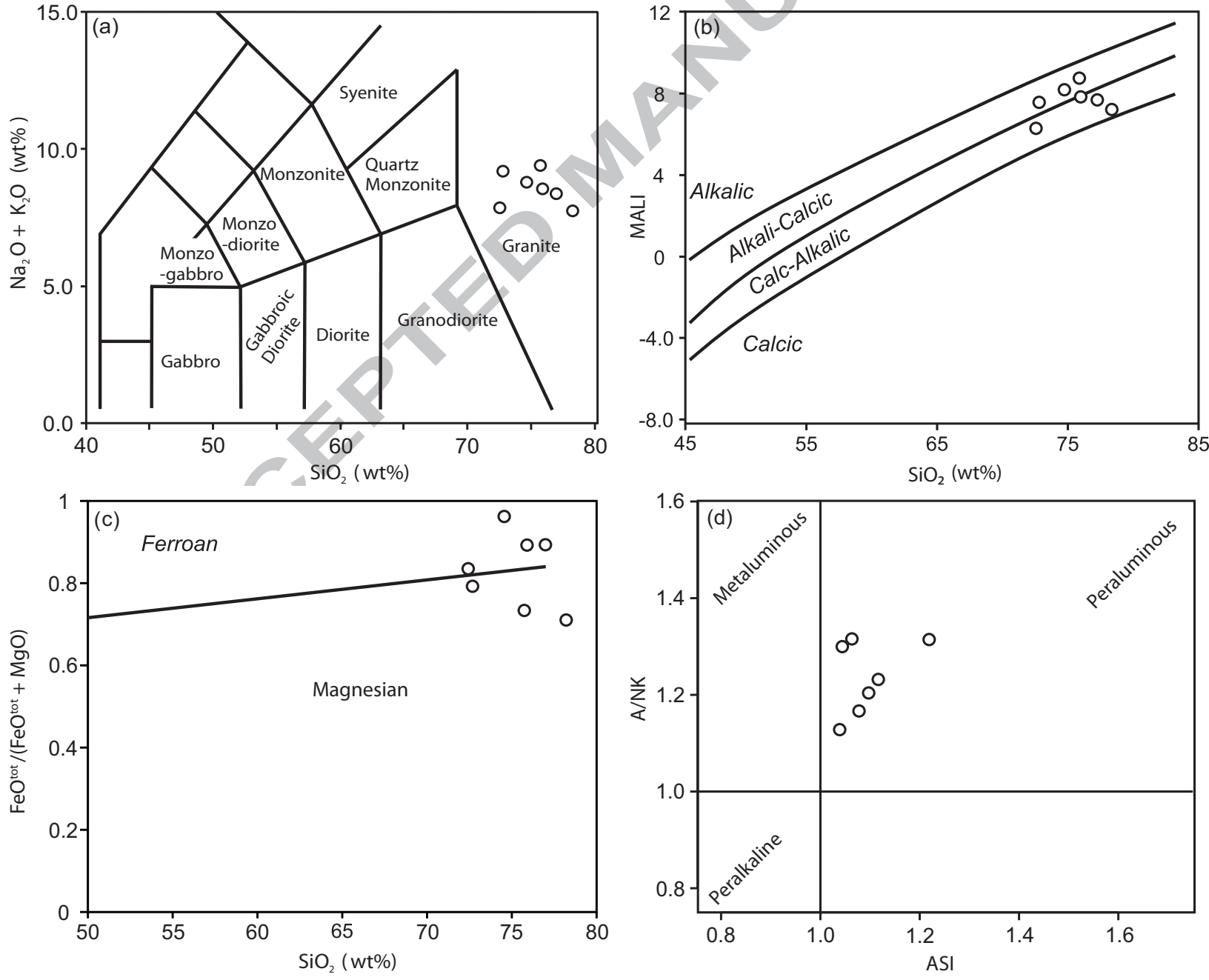

Figure 8

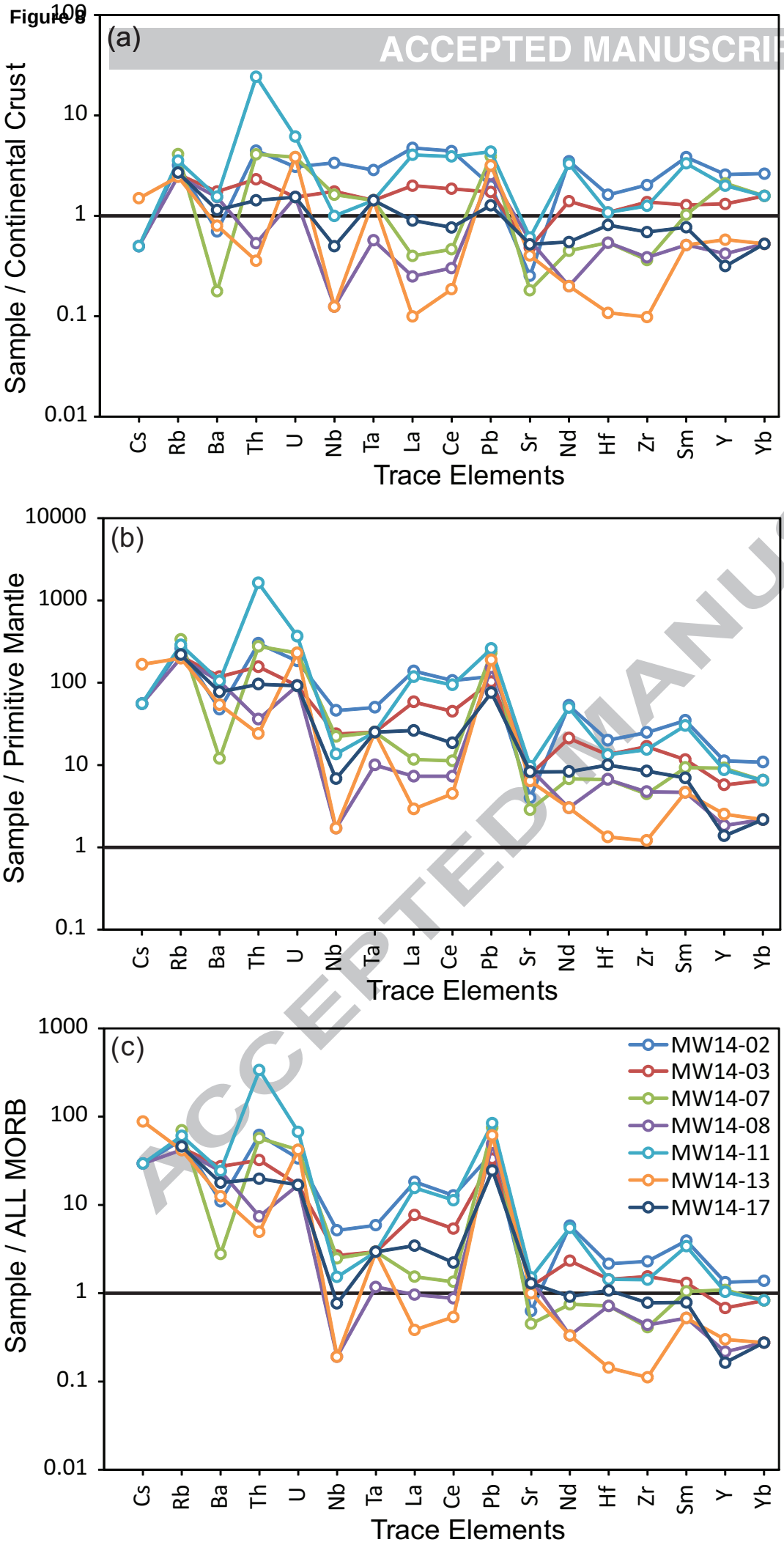

Figure 9

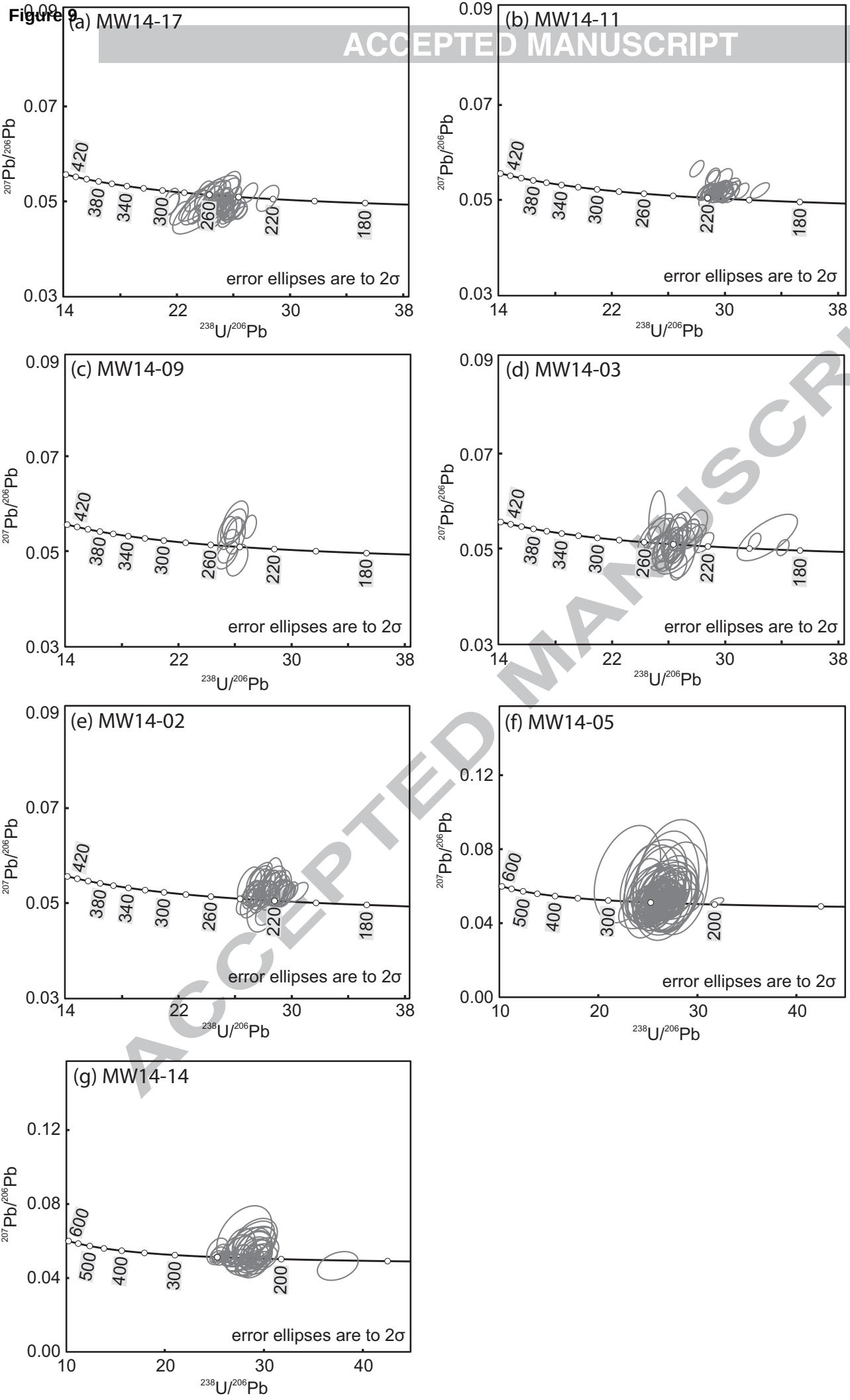

Figure 10

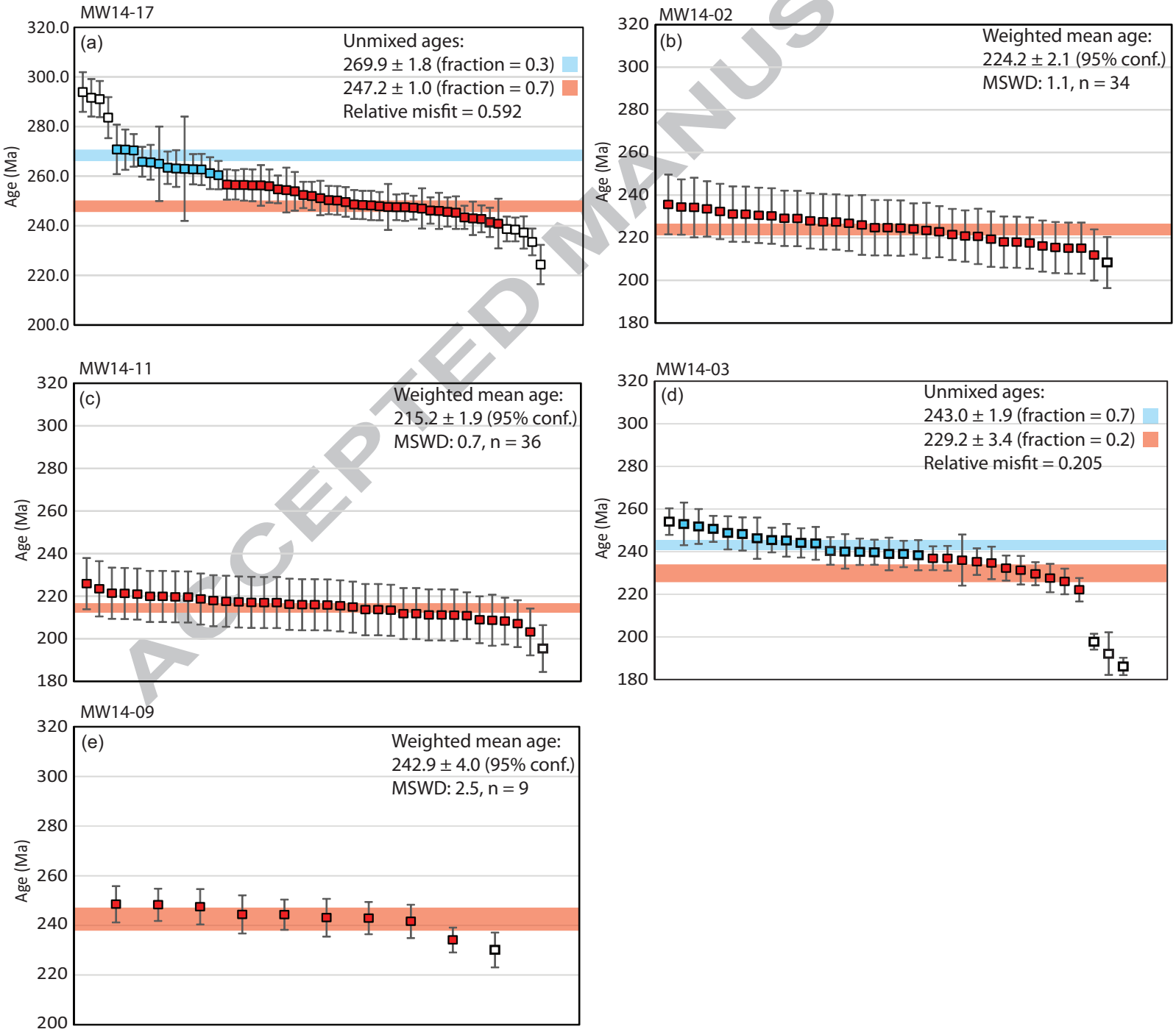

Figure 11

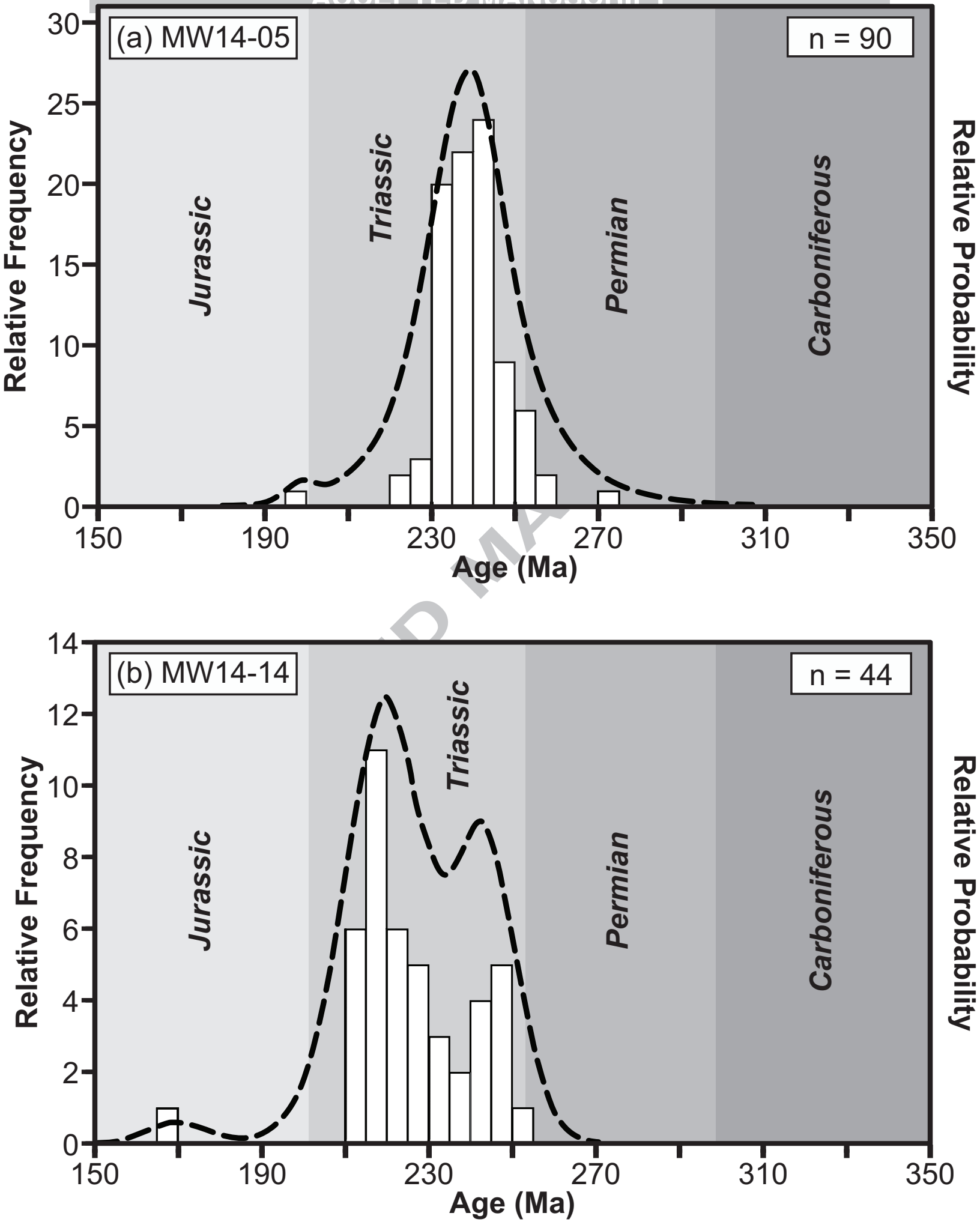

Figure 12

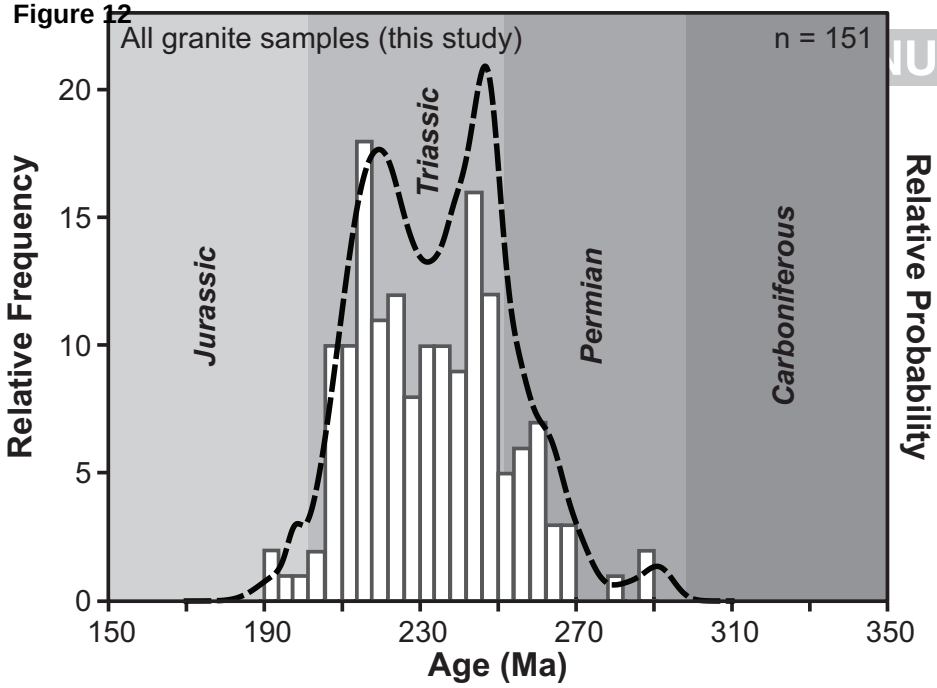

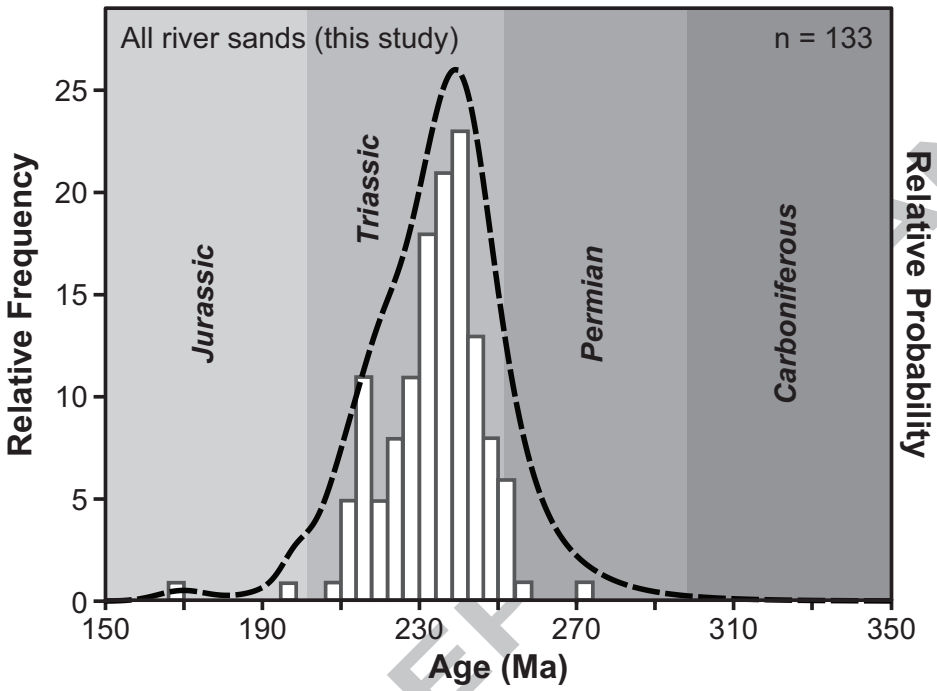

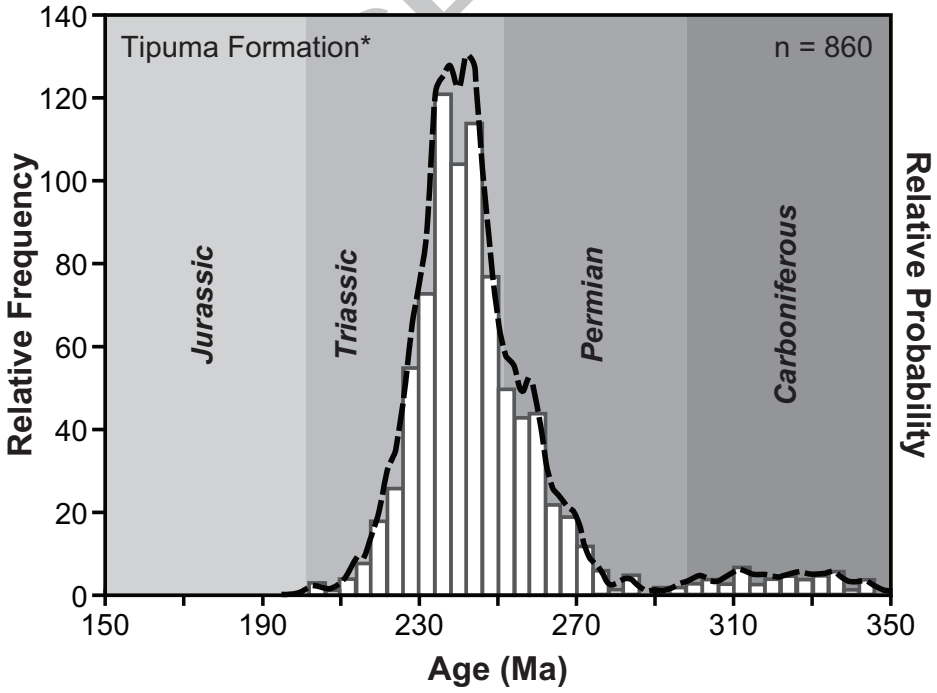

Figure 13

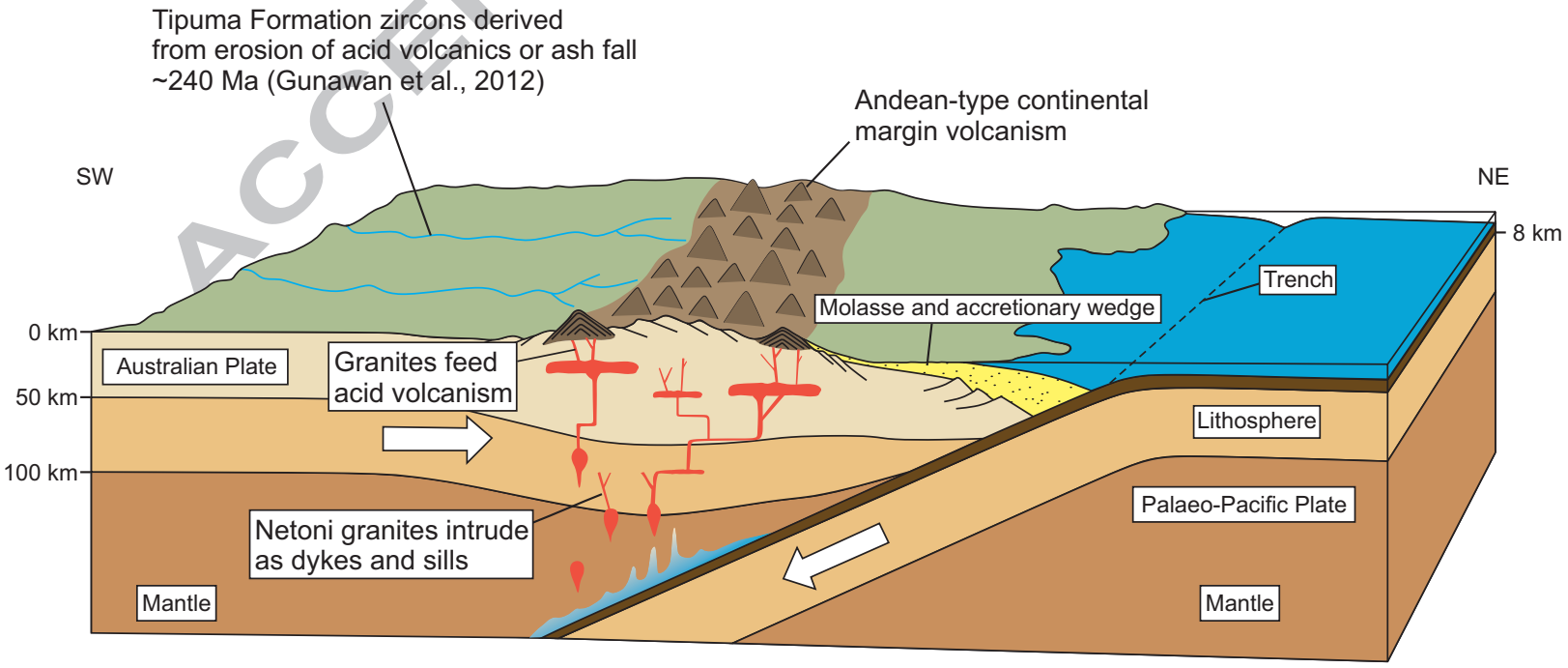

Bird's Head Peninsula at ~240 Ma

Graphical abstract

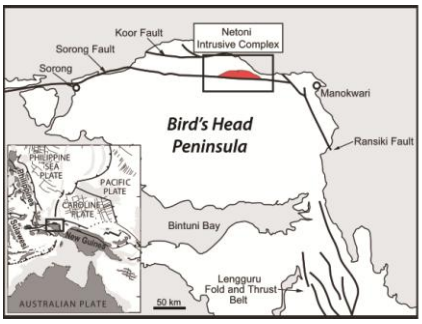

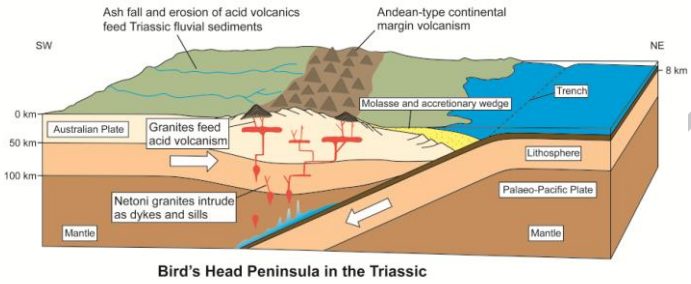

Bird's Head Peninsula in the Triassic

Research Highlights:

- We report geochemistry, petrography and geochronology for granites in West Papua.
- Alkali-calcic to calc-alkali granites formed during the Triassic (248-213 Ma).
- These were emplaced in a continent-arc subduction setting along eastern Gondwana.
- Erosion of which may be a source for Triassic zircons in sediments from West Papua.